António José Ribeiro Simões

Ring-type Magnitude Modulation for LINC: Paving the road for better efficiency

Setembro de 2014

· U C ·

UNIVERSIDADE DE COIMBRA

Ring-type Magnitude Modulation for LINC: Paving the road for better efficiency

António José Ribeiro Simões

Dissertação para obtenção do Grau de Mestre em

Engenharia Electrotécnica e de Computadores

Orientador: Doutor Marco Alexandre Cravo Gomes
Co-Orientador: Doutor Vítor Manuel Mendes da Silva

Júri

Presidente: Doutora Teresa Martinez dos Santos Gomes
Orientador: Doutor Marco Alexandre Cravo Gomes
Vogais: Doutor Rui Miguel Henriques Dias Morgado Dinis
Doutor Rui Pedro Duarte Cortesão

Setembro de 2014

In any case you mustn't confuse a single failure with a final defeat.
- F. Scott Fitzgerald, Tender is the Night

Aye, I suppose I could stay up that late.
- James Clerk Maxwell
(On being told on his arrival at Cambridge University that
there would be a compulsory 6 a.m. church service.)

Agradecimentos

Este trabalho surge no culminar do meu percurso académico de cinco anos, para o qual pude contar com diversas contribuições. Quero, por isso, aproveitar esta oportunidade para agradecer a todos os que me apoiaram ao longo destes anos.

Começo por agradecer ao Instituto de Telecomunicações, por me ter acolhido e por todos os meios materiais disponibilizados, e à Fundação para a Ciência e Tecnologia, por ter financiado em parte este trabalho.

Aos meus colegas de laboratório, pelo espírito de entreajuda e por toda a boa disposição e motivação que trouxeram consigo diariamente, proporcionando assim um ambiente de trabalho sem paralelo.

Aos meus colegas de curso, pelos momentos que passámos nestes últimos cinco anos.

Ao Professor Rui Dinis, pela motivação e entusiasmo que trouxe a este trabalho.

Aos meus orientadores, o Professor Marco Gomes e o Professor Vitor Silva, pela paciência e vontade de partilha de conhecimento que traziam consigo nas horas de discussão deste trabalho, e pelo esforço e disponibilidade que mantiveram até ao último minuto.

Aos meus amigos, com quem eu posso sempre contar.

E por último, um agradecimento especial aos meus pais, ao meu irmão e à minha avó, pela incomparável disponibilidade e vontade de me ajudarem a atingir os meus objetivos, e pela entrega e presença em todas as etapas da minha vida.

A todos,
Muito Obrigado.

Abstract

The rising demand for energy efficiency, namely on the uplink channel, is severely restricted by the linear input-output power amplification requirements, which is normally performed by linear high power amplifiers (HPAs). To overcome the necessity of using these inefficient amplifiers, a linear amplification with nonlinear components (LINC) technique was developed. This technique separates each input signal in two constant-envelope branches, to be amplified separately by grossly non linear (NL) HPAs, which are simpler and much more energy efficient than the linear ones. However, the wide spectrum of the LINC signal components limits this technique's potential efficiency, restricting the combiner's efficiency, raising the necessary oversampling rate and requiring a larger bandwidth for the HPAs to accommodate.

To address this problem, this thesis work developed a new ring-type magnitude modulation (RMM) method to control the transmitted signal's envelope excursions. This look-up table (LUT) based magnitude modulation (MM) method was specially thought for offset modulations schemes like offset quadrature phase shift keying (OQPSK), and enforces lower and upper amplitude boundaries on the transmitted signal's envelope.

Results show that combining the proposed RMM method to the LINC transmitter effectively reduces the LINC signal components' bandwidth, and thus successfully reduces the system's oversampling requirements and increases the combiner's energy efficiency. This method was also shown to be fairly insensitive to small gain and phase imbalances between the HPAs' gains.

Keywords

LINC, RMM, OQPSK modulation, Energy efficiency, Signal Processing

Resumo

O crescente interesse por eficiência energética, sobretudo no sentido de transmissão ascendente (*uplink*), é fortemente limitado pelos requisitos de amplificação linear de potência, que normalmente é efectuada por amplificadores de alta potência (HPA). Para superar a necessidade de utilizar estes amplificadores de baixa eficiência, foi desenvolvida uma técnica de amplificação linear com componentes não lineares (LINC). Esta técnica separa um dado sinal em dois sinais de envolvente constante, para serem amplificados recorrendo a HPAs não lineares, que são mais simples e muito mais eficientes do ponto de vista energético do que os HPAs lineares. Porém, esta operação de separação do sinal provoca um alargamento do espectro das duas componentes LINC, e acaba por restringir o potencial desta técnica, já que limita a eficiência do combinador, aumenta a taxa de sobreamostragem mínima e requer a utilização de HPAs que tenham capacidade de acomodar esta maior largura de banda.

Para enfrentar este problema, nesta trabalho de tese foi desenvolvido um novo método de modulação de magnitude em anel (RMM), para controlar as excursões da envolvente do sinal transmitido. Este método de MM baseado em tabelas de consulta (LUT) foi desenvolvido considerando os esquemas de modulação com desfasamento temporal, como o OQPSK, e limita inferior e superiormente a envolvente do sinal transmitido.

Os resultados mostram que da combinação do método RMM proposto com o transmissor LINC resulta uma redução efetiva da largura de banda dos sinais que compõem o LINC, e desta forma consegue-se reduzir os requisitos relativos à taxa de sobreamostragem e aumentar a eficiência energética do combinador. Também se verifica que este método é razoavelmente insensível a pequenos desvios de fase e amplitude entre o ganho de potência dos HPAs.

Palavras Chave

LINC, RMM, Modulação OQPSK, Eficiência energética, Processamento de Sinal

Contents

Contents

List of Figures

List of Figures

List of Tables

List of Tables

List of Acronyms

AWGN	additive white gaussian noise
BER	bit error rate
CDF	cumulative distribution function
DAC	digital-to-analog converter
FIR	finite impulse response
FPGA	field programmable gate array
HPA	high power amplifier
IB-DFE	iterative block decision feedback equalisation
LDPC	low-density parity-check
LINC	linear amplification with nonlinear components
LUT	look-up table
MC	multi-carrier
MM	magnitude modulation
MPMM	multistage polyphase magnitude modulation
NL	non linear
OQPSK	offset quadrature phase shift keying
PAPR	peak-to-average power ratio
PC	polar clipping
PDF	probability density function

List of Tables

PS   polar scaling

PSD   power spectral density

QPSK   quadrature phase shift keying

RC   rectangular clipping

RMM   ring-type magnitude modulation

RRC   root raised cosine

RS   rectangular scaling

SC   single-carrier

1

Introduction

Contents

1. Introduction

The rising demand for spectral and power efficiency in communication systems, namely on mobile devices, makes the study of low peak-to-average power ratio (PAPR) signals worthy of attention, in order to lower requirements of back-off from the high power amplifier (HPA) saturation point [1–4]. The HPA is one of the critical components in the design of wireless transmitters, to which most spectral efficient transmission techniques impose stringent linearity requirements (i.e., the use of class A or AB power amplifiers or quasi-linear amplifiers) with a consequent negative impact on power efficiency (e.g., class A power amplifiers' efficiency is below 20%) and HPA's cost.

With this in mind, the use of the linear amplification with nonlinear components (LINC) [5–7] technique becomes attractive, since this structure separates the input signal in two constant-envelope branches to be amplified separately by two highly efficient grossly non linear (NL) amplifiers (e.g., class D and E amplifiers, whose efficiencies reach 80%), which are simpler, cheaper and have higher amplification than quasi-linear amplifiers [4,8]. A linear amplified replica of the input signal is obtained by combining the two amplified component signals as long as the amplifiers are perfectly matched (i.e. without gain and phase imbalances between each other) [5, 6] and have sufficient bandwidth to accommodate each LINC component signal.

Along with the HPA, the LINC's combining structure plays a critical role in the transmitter's overall power efficiency [6, 9]. As explained in the next chapter, decreasing the transmitted signal's PAPR generally also results in an increase on the combiner's average power efficiency [9].

Besides distortions due to imperfect combining, the LINC scheme may also involve amplitude clipping due to input power limitations of the component amplifiers, which would result in additional high frequency distortion (i.e. spectral regrowth) on the transmitted signal [10]. To avoid the mentioned distortion, the signal should remain below the amplitude clipping level as often as possible. But this clipping level should not be feared, since it can provide an important tradeoff between power and spectral efficiency when used with caution.

Caution brings back the signals' high PAPR problem, but this time for a different reason. Suppressing the peaks from the transmitted signal would result in fewer signal amplitude clipping occurrences, which would mitigate the undesirable high frequency distortion that it adds on the reconstructed signal. In this context, the magnitude modulation (MM) techniques [11–13] are known to be effective methods of controlling the signal's envelope excursions without spreading the transmitted signal's spectrum, and noticeably reducing the transmission performance.

One of the challenges of the LINC transmitter regards its oversampling requirements [7]. The two LINC branches have a larger spectrum than the input signal (consistent

with the wide characteristic of the spectrum of a constant envelope signal [6]), since each branch's generation results from performing a phase modulation procedure of the input signal's amplitude, to be described in chapter 2. However, a smaller amplitude range would result in a smaller phase modulation effect, which would narrow the branch's spectrum. On such conditions, using an offset type of modulation scheme should provide good results [6, 9]. Therefore, a new MM method should be designed to fit these LINC transmission requirements.

After this analysis it became clear how relevant it would be to study the resulting effect of including a peak power control technique in a LINC transmission system, with the purpose of exploring its potential benefits, namely regarding spectral and power efficiency.

1.1   Objectives

The core of this thesis work is to study the impact of an MM scheme on a single-carrier (SC) LINC transmission system. It is proposed a new MM method for an offset quadrature phase shift keying (OQPSK) modulation scheme[1], specially designed to be combined with a LINC transmitter (namely to reduce its oversampling requirements). It is also explored the possible tradeoffs that result from properly choosing the values for this system's set of parameters.

In order to correctly compare the different transmission schemes considered, the analysis is focused on four criteria:

- the LINC branches' power spectral density (PSD), as a measure of its oversampling requirements,

- the transmitted signal's PSD, to assess the spectral regrowth of this signal's bandwidth,

- the distribution of the decomposition angle θ of the LINC branch's constant envelope signal, which provides the necessary information on the system's overall power efficiency,

- the system's bit error rate (BER), in order to evaluate its performance.

The proposed schemes' entire simulation set was developed using the Matlab® environment [14], namely the *Communications System Toolbox*.

---

[1]More information regarding this digital modulation scheme on appendix A.

1.2   Dissertation Outline

This thesis is structured in five chapters. Following the introduction, Chapter 2 will provide an overview on the LINC transmission system, where careful attention is payed to the benefits and limitations that it imposes on the overall communication system. Chapter 3 focuses on the MM principles, and explains a few methods to employ this technique in transmission systems. It also presents the proposed MM scheme. Chapter 4 analyses the magnitude modulated LINC scheme, regarding the four criteria aforementioned. Finally, Chapter 5 discusses the main conclusions drawn from this thesis work, and reflects on the possible paths for future work on this subject.

1.3   Thesis framework and contributions

This thesis work was carried out under the projects GALNC [15] (Generalized Linear Amplification with Nonlinear Components for broadband wireless systems (EXPL/EEI-TEL/1582/2013), funded by Fundação para Ciência e Tecnologia – FCT) and GLANCES [16] (Generalized Linear Amplification with Nonlinear Components for Power and Spectral Efficient Broadband Wireless Systems, supported by Instituto de Telecomunicações – IT).

From the early stage of this work has resulted the paper attached to appendix B, which was accepted for oral presentation at IEEE 80th Vehicular Technology Conference 2014. The latest developments lead to two provisional applications for patents, regarding the developed MM scheme [17] and the MM combined with LINC efficient transmitter scheme [18].

2

LINC systems

Contents

In numerous communication systems it is required to have a linear input-output power relationship. This requirement brings a great restraint on the choice of HPAs to include in such systems, because the linear type HPAs have a substantially lower energy efficiency [4, 8]. The LINC technique [5–7] was developed to overcome the linearity imposed restraints, managing to achieve linear power amplification while employing highly efficient and grossly NL HPAs.

On that note, this chapter describes the basic concepts of the LINC technique. The many challenges that this system faces nowadays are also discussed, in order to provide the needed background to understand the proposed scheme.

2.1 LINC basic concepts

Using vector decomposition, it is possible to separate any two-dimensional signal in two constant-envelope signals by mapping the desired information in each of their phases, as illustrated by figure 2.1. This is the basic idea behind the LINC technique.

(a) LINC representation using θ. (b) LINC representation using $e(t)$.
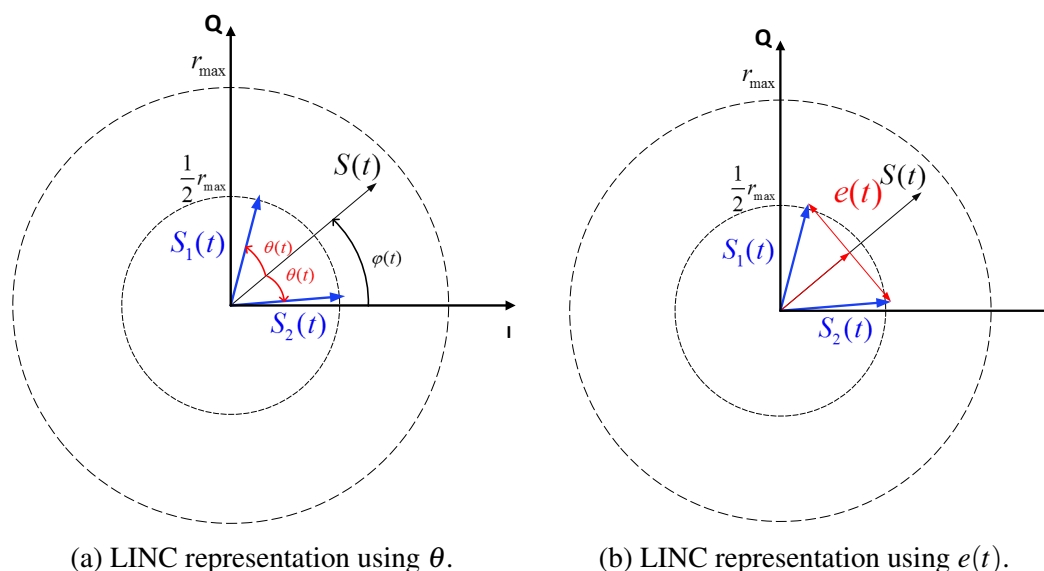
Figure 2.1: Signal separation operated by the LINC system, based on vector decomposition.

A generic communication signal $S(t)$, both for SC and multi-carrier (MC) communications, can carry information in both amplitude and phase, and can be generically represented by

$$S(t) = r(t)e^{j\phi(t)} \, , \tag{2.1}$$

where $r(t) \geq 0$ and $\phi(t)$ represent respectively the instantaneous signal's magnitude and phase, that can be time-varying functions. The mathematical representation of the LINC

concept becomes clear by replacing the signal's magnitude $r(t) = r_{max}cos(\theta(t))$ in equation (2.1), i.e. by representing $r(t)$ as a constant amplitude phase modulated signal, where r_{max} is its maximum amplitude and $\theta(t)$ is the LINC branches' decomposition angle, as depicted in Fig. 2.1a.

Using the exponential representation of $cos(\theta(t))$, equation (2.1) can be rewritten as:

$$S(t) = \frac{r_{max}}{2}e^{j\phi(t)}\left(e^{j\theta(t)} + e^{-j\theta(t)}\right) . \tag{2.2}$$

Finally, equation (2.2) can be further simplified to $S(t) = S_1(t) + S_2(t)$, where:

$$S_1(t) = \frac{r_{max}}{2}e^{j(\phi(t)+\theta(t))} , \tag{2.3}$$

$$S_2(t) = \frac{r_{max}}{2}e^{j(\phi(t)-\theta(t))} , \tag{2.4}$$

proving that any signal $S(t)$ can be written as a sum of constant amplitude signals.

Representing the LINC branches' using equations (2.3) – (2.4) is a very powerful way to evaluate the transmission system's overall power efficiency, due to the close connection between this efficiency and the decomposition angle $\theta(t)$ (as it will be discussed later in this chapter). However, there is an equivalent set of equations to describe the signal separation, as follows:

$$S_1(t) = \frac{1}{2}S(t)(1 + je(t)) , \tag{2.5}$$

$$S_2(t) = \frac{1}{2}S(t)(1 - je(t)) , \tag{2.6}$$

with $e(t) = \sqrt{\left(\frac{r_{max}}{r(t)}\right)^2 - 1}$, which can be obtained with a simple inspection of fig. 2.1b. A simple analysis confirms that, in both cases, the two branches have equal and constant amplitude $\frac{s_M}{2}$, making it possible to include two grossly NL amplifiers on this transmission system without distortion. These amplifiers are inexpensive and much more energy-efficient than the linear ones [4, 8].

Although equations (2.3) – (2.4) and (2.5) – (2.6) are mathematically equivalent[1], one set of the equations may outperform the other in a given digital implementation of this system, depending on how the signal separation process is physically handled [6, 19, 20]. However, this analysis is out of the scope of this thesis work.

---

[1]The two notations will be used interchangeably, depending on which representation fits each analysis better.

2.2 Digital LINC transmission system

Following this analysis, the basic digital LINC transmitter is presented in figure 2.2.
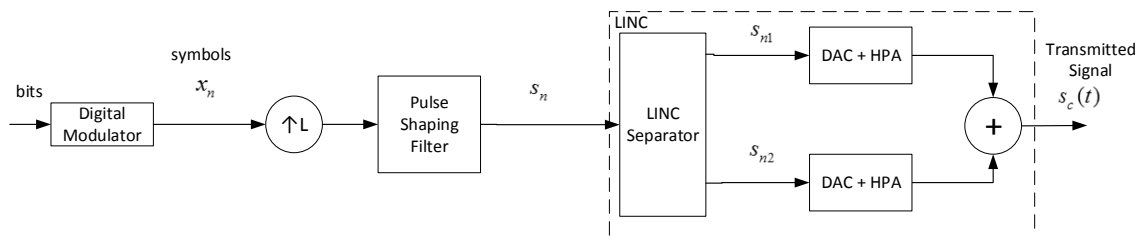
Figure 2.2: Basic digital LINC transmission system.

Due to the flexibility offered by digital signal processing, LINC separation is usually on the digital domain [6,19,20], as well as bandwidth limiting by pulse shaping (normally an RRC filter [21]), which is performed before the LINC technique.

Although equations (2.1) – (2.6) are straightforward to convert to its discrete-time equivalent, some care must be taken regarding the required oversampling rate.

In order to keep the constant-envelope characteristic of the LINC signal components s_{n1} and s_{n2}, it is necessary to account for their wide spectrum when designing the DAC's reconstruction filter, to ensure negligible peak regrowth on those signals. This design can be made simpler by using a higher oversampling rate, allowing a considerable reduction in the reconstruction filter's order, and so lowering its cost [21].

Therefore, a digital domain analysis needs to take in consideration the digital-to-analog converter (DAC) features (resolution and reconstruction filter characteristics) and the HPAs' saturation effect in the discrete-time representation of $\theta(t)$ and $e(t)$, which may require the clipping of the LINC's input signal s_n. Accordingly, the digital representation of θ and e is given by:

$$\theta(r_n) = \begin{cases} \arccos\left(\frac{r_n}{s_M}\right), & r_n \leq s_M \\ 0, & r_n > s_M \end{cases}, \tag{2.7}$$

$$e(r_n) = \begin{cases} \sqrt{\left(\frac{s_M}{r_n}\right)^2 - 1}, & r_n \leq s_M \\ 0, & r_n > s_M \end{cases}, \tag{2.8}$$

where r_n is the magnitude of the original signal at sample n and s_M is the mentioned LINC transmission system's clipping level. This polar clipping operation is usually chosen over the Cartesian type due to its slightly superior performance [7]. Assuming ideally balanced amplifiers and perfect combining, we can determine the transmitted signal s_c using the following equation (where it is assumed an amplifiers' unit power gain):

$$s_c = s_{n1} + s_{n2} = \begin{cases} s_n, & |s_n| \leq s_M \\ s_M e^{j \ \arg(s_n)}, & |s_n| > s_M \end{cases}. \tag{2.9}$$

Besides sufficient bandwidth to accommodate each signal's component, this system requires the mentioned perfectly balanced HPAs in order to cancel the complementary terms of s_{n1} and s_{n2} (check equations (2.5) – (2.6) for simplicity). Hence, possible amplitude or phase unbalances between the two amplifying branches may result in significant performance degradation [6, 7]. This question will be addressed in chapter 4.

In the next sections it will be discussed some of this system's feature regarding the LINC's separator and combiner structures, respectively.

2.2.1 LINC's separator structure

One of the main challenges that the LINC transmission system faces has to do with the signal separation process. The nonlinear operation portrayed by either applying the equations (2.7) or (2.8) to obtain s_{n1} and s_{n2} results in an increase of the LINC branches' bandwidth relative to the original signal's [6]. This out of band spectral regrowth occurs because of the added phase modulation depicted in the time-discrete version of equations (2.3) – (2.4).

In order to enable perfect recombination, this bandwidth enlargement needs to be accommodated by the HPAs and the DACs' reconstruction filter. This can be handled by working the system at a higher sample rate. With this in mind, figure 2.3 illustrates the mentioned out of band spectral regrowth effect on both LINC branches' bandwidth[2] when the information is mapped in QPSK and OQPSK constellations, respectively. While a high oversampling factor ($L \geq 16$) is critical for a feasible transmission system using QPSK, this factor is much less restrictive when it is used an OQPSK digital modulator ($L = 8$ results in a simpler reconstruction filter design), due to the lower HPAs' bandwidth requirements for the LINC signal components of the OQPSK signal. This constraints will be taken into account in the following chapters when choosing the transmission system's parameters.

2.2.2 LINC's combiner structure

As mentioned before, the main advantage of choosing a LINC transmission system over one with linear HPAs is its potentially higher energy efficiency, since it can employ grossly NL HPAs. However, in order to correctly evaluate the entire transmission system

---

[2]It is enough to analyse only one of the branches, since they have similar amplitude response.

(a) QPSK modulation.

(b) OQPSK modulation.
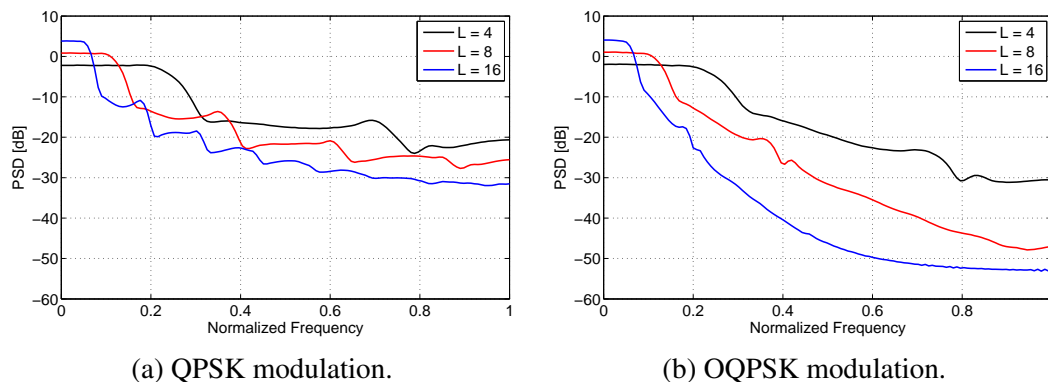
Figure 2.3: LINC branch's PSD for different oversampling factors L – the RRC filter has a 25% roll-off factor.

one must consider the combiner structure's role in it. As [6] states, the combiner's energy efficiency is closely related to the decomposition angle θ, as follows:

$$\eta_{comb} = \cos^2 \theta . \tag{2.10}$$

Since the decomposition angle is likely to change during the transmission time (recall equation (2.7)), equation (2.10) alone does not provide a full insight of the problem, making it necessary to instead estimate the combiner's average energy efficiency that considers the decomposition angle's distribution:

$$\overline{\eta}_{comb} = \int_0^{\pi/2} pdf_{sinal}(\theta) \times \cos^2(\theta)d\theta . \tag{2.11}$$

To complete this preliminary analysis, figure 2.4 illustrates the average LINC combiner's energy efficiency when it is used QPSK and OQPSK digital modulators[3]. Such a system would be terribly inefficient, since most of the signal's decomposition angle is concentrated between $30°$ and $70°$ degrees, while completely wasting the "efficient angles".

---

[3]Neither signal was clipped, to simplify this introductory analysis.
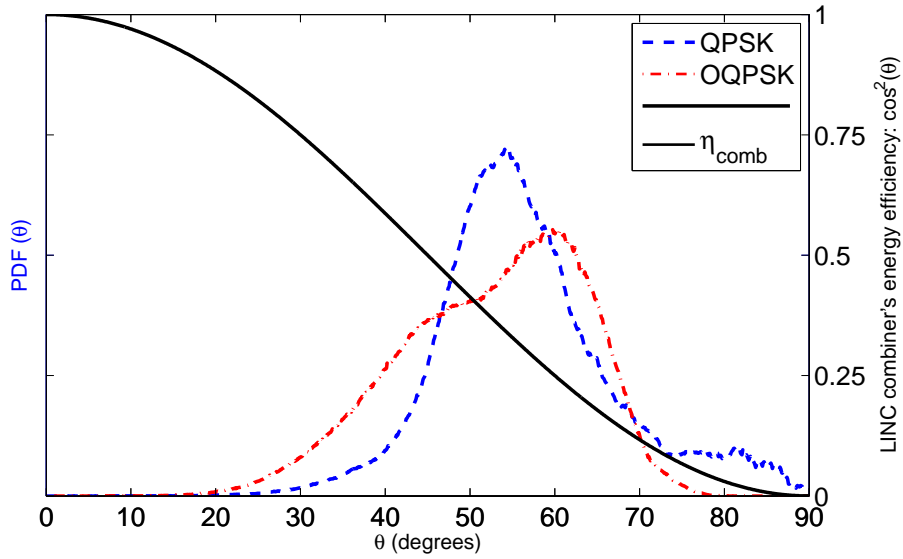
Figure 2.4: QPSK and OQPSK's decomposition angle θ vs LINC combiner's efficiency.

A simple inspection on equation (2.7) shows that one of the ways to improve the combiner's average energy efficiency is to lower the LINC's clipping level s_M, but it would deteriorate the system's performance, since post-filtering PAPR reduction techniques may cause spectral spreading, thus causing loss of bandwidth efficiency and undesirable adjacent channel interference [12]. However, there are more appropriated ways to achieve the desired effect, like controlling the envelope excursions of the signal fed to the LINC system, that will be explained in the next chapter.

3

Magnitude Modulation

Contents

Typical SC transmitters work with linear HPAs, whose input back-off requirements greatly reduce the system's energy efficiency. In this context, magnitude modulation techniques were developed to control envelope excursions of the transmitted signals by adjusting each symbol prior to filtering. Such an adjustment takes into account the pulse shaping filter (typically a RRC) impulse response, since it is the main cause for the mentioned envelope excursions[1]. One of the benefits of these schemes comes from the fact that they do not enforce a penalty reduction in the information rate, while effectively increase the transmitter's energy efficiency [13, 22]. The same reasoning can be applied in order to find a solution for the constraints described in section 2.2.2.

This chapter presents a new MM technique specially thought to fit the LINC transmission system's requirements, namely regarding its overall energy efficiency. This new method employs a polar clipping-rectangular scaling approach [11, 12] on OQPSK signals, and it makes use of a LUT (computed *a priori*) to provide each symbol's MM coefficients, according to its neighbors. The needed background for this MM scheme is provided in the following sections, where it is studied this technique's state of the art, namely regarding implementations of this method on QPSK signals.

Initially, the new method's performance is evaluated in a SC transmission scheme alongside the computation of the decomposition angle θ that would be obtained if the transmitted signal was included in a LINC transmitter instead without performing amplitude clipping, to allow a fair comparison between the different scenarios. After choosing the most favorable set of parameters, this evaluation proceeds to chapter 4, where this technique is included in the LINC transmission scheme seen in figure 2.2.

3.1   The Magnitude Modulation Principle

Figure 3.1 presents a typical SC transmitter, with the basic building blocks to enable a successful communication. As it was mentioned before, when the transmitted symbols are mapped in constant-envelope constellations, the main contribution for high PAPR on the transmitted signal comes from the pulse-shaping filter (normally RRC). Taking this into account, a symbol readjustment procedure could be employed prior to filtering to reduce the signal's envelope excursion. This is the basic concept of the MM method, similar to the adaptive peak-suppression algorithm for M-PSK type constellations proposed by Miller *et al.* [1].

Figure 3.2 illustrates the MM principle. Despite the different ways to apply this method, each MM implementation is composed of the following steps:

---

[1]The other contribution comes from the symbol constellation itself. However, this work only deals with constant envelope constellations, that have a 0 dB PAPR contribution to the transmitted signal [22].
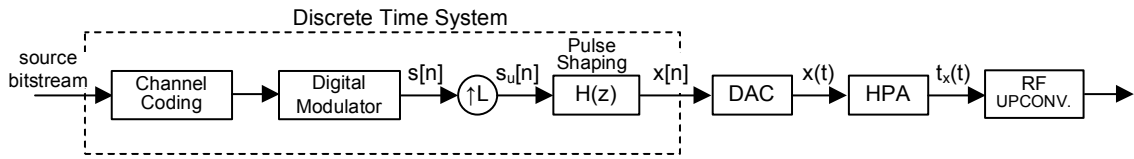
Figure 3.1: Generic SC transmitter scheme [12].

- Predicting the response of the pulse shaping filter to a given symbol sequence $s[n]$ (depending on the filter length).

- Detect the peaks of the predicted response and calculate the corresponding scaling factor.

- Multiplying the symbol[2] s_n by its MM coefficient m_n.
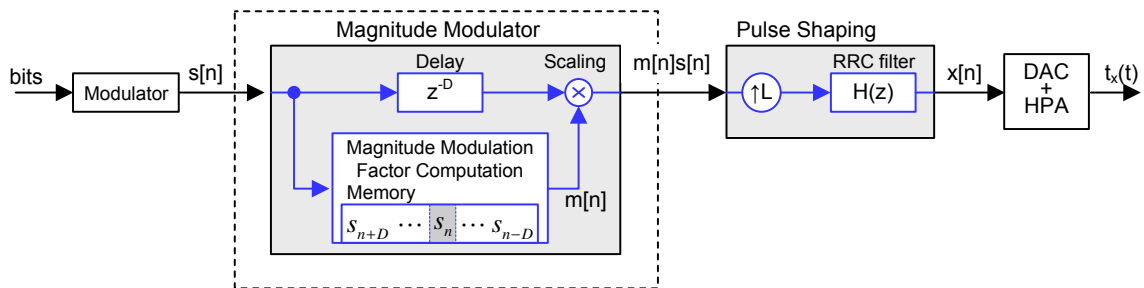
Figure 3.2: Magnitude modulation principle [12, 22].

In order to correctly compute each symbol's MM coefficient it is necessary to consider the RRC filter's length, to account for all the symbols that significantly contribute to the signal's amplitude (seen in figure 3.2 as the D past and future neighbors of the highlighted symbol). Therefore, this operation inserts a small time delay DT_{symb}, where T_{symb} is the symbol's duration.

In the peak detection step, there are two possible criteria to enforce: polar clipping (PC) and rectangular clipping (RC). When polar clipping is employed, the MM coefficient to be applied to s_n considers the amplitude of the predicted response sequence and compares it to a given threshold A, whereas a rectangular clipping type of approach evaluates the in-phase and quadrature components separately, with threshold levels A_I and A_Q, respectively

The scaling operation follows a similar reasoning. A rectangular scaling (RS) approach scales the in-phase and quadrature symbol components separately (i.e. each symbol needs two MM coefficients, one for each symbol component), as follows:

---

[2] s_n refers to the particular sample at instant n, where $s[n]$ regards the discrete time sequence. The same notation is applied to the MM coefficients.

$$x[n] = \left[\sum_k m^I[k] \, s^I[k] \, \delta[n-kL]\right] * h[n] + \left[\sum_k m^Q[k] \, s^Q[k] \, \delta[n-kL]\right] * h[n] \ . \qquad (3.1)$$

On the other hand, a method using PS multiplies each symbol s_n with one coefficient m_n:

$$x[n] = \left[\sum_k m[k] \, s[k] \, \delta[n-kL]\right] * h[n] \ . \qquad (3.2)$$

Despite adding some phase modulation, an RS approach can provide a finer control of the envelope excursions over the other method, since it has an additional degree of freedom.

The following subsections explore the method's developed by Tomlinson *et al.* [11] and [12], and how they applied the aforementioned steps.

3.1.1 Look-Up Table Based Approach

In 2002, Tomlinson *et al.* [11] proposed a MM scheme where the MM coefficients are computed *a priori* and stored in a look-up table (LUT)[3], as generally depicted in figure 3.3. In order to magnitude modulate a given symbol, it is only necessary to search the LUT for the shift register's state, and fetch the corresponding coefficient(s) (depending on whether PS or RS is employed), since this table contains all possible states.
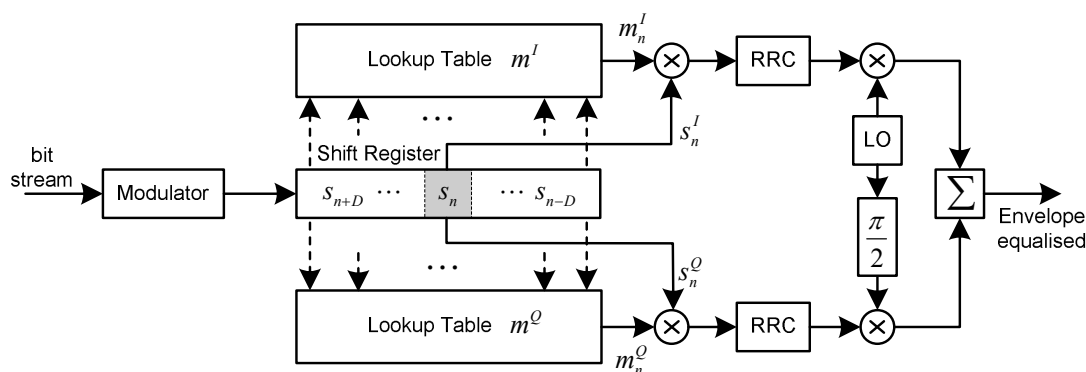
Figure 3.3: Generic LUT-based Magnitude Modulation transmitter scheme [11, 12].

The MM coefficients to be stored in the look-up table are estimated according to the iterative algorithm 1, where noiseless transmission is emulated. This algorithm is thoroughly illustrated in figure 3.4, including the different clipping and scaling preferences[4].

---

[3]Figure 3.3 employs rectangular scaling. An equivalent PS approach would only have one look-up table.
[4]The algorithm's analysis is supported by this figure's notation.

Algorithm 1 Concise Algorithm for Computation of MM Coefficients' LUT [12].

---

do {

    STEP 0*:* **Setup input data.**

$$Input\ Data = \begin{cases} Signal\ to\ be\ MM & \Leftarrow & \text{first iteration} \\ MM\ signal\ from\ previous\ iteration & \Leftarrow & \text{other iterations} \end{cases}$$

    STEP 1*:* **Filter data using a RRC filter.**

    STEP 2*:* **Limit the magnitude of the filtered signal to the specified threshold** A**.**

    STEP 3*:* **Filter the resulting signal using a match RRC filter.**

    STEP 4*:* **Sample the resulting signal to obtain the MM sequence corresponding to the input data.**

} **while** (Signal limitation occurs in *STEP* 2)

    STEP 5*:* **Output the MM coefficients by performing the ratio of MM signal from the most recent iteration to the input original sequence to be MM.**

Initially, each MM coefficients sequence is an all ones vector, so that the algorithm's first iteration does not include MM. After upsampling and RRC filtering the input sequence $a[n]$, the resulting signal $y[n]$ is evaluated according to the algorithm's clipping method. Then, the clipped signal is fed to a matched RRC filter, and sampling is performed on the received signal to obtain the symbols corresponding to the input data. Finally, the ratio between each received symbol $a_{Rx}[n]$ and the original sequence $a[n]$ is calculated and stored in the respective slot of the coefficient stream $m[n]$, and the algorithm is repeated with this new MM factors until no further clipping is enforced in step 2. When the algorithm stops, the coefficient[5] m_0 is stored in the look-up table at the position defined by the corresponding state.

There are a few remarks to be made about the LUT computation procedure. First of all, it should be stressed that the neighboring symbols' MM coefficients are updated at the end of each iteration, in order to account for their MM's distortion contribution to the signal's envelope on the final value of m_0.

In order to speed-up the computation of the look-up table (LUT), the algorithm should include an alternative stopping criteria that ensures convergence, since infinite loop situations may occur. The work developed in [12] suggests monitoring the peak value of $y[n]$ and stopping if it is in the close vicinity of the threshold A at some point and it doesn't

---

[5]For simplicity, the algorithm analysis is made as if it was employed polar scaling and polar clipping. Whichever commentaries are made regarding m_0 are equally valid on m_0^I and m_0^Q, if RS is used instead of PS.
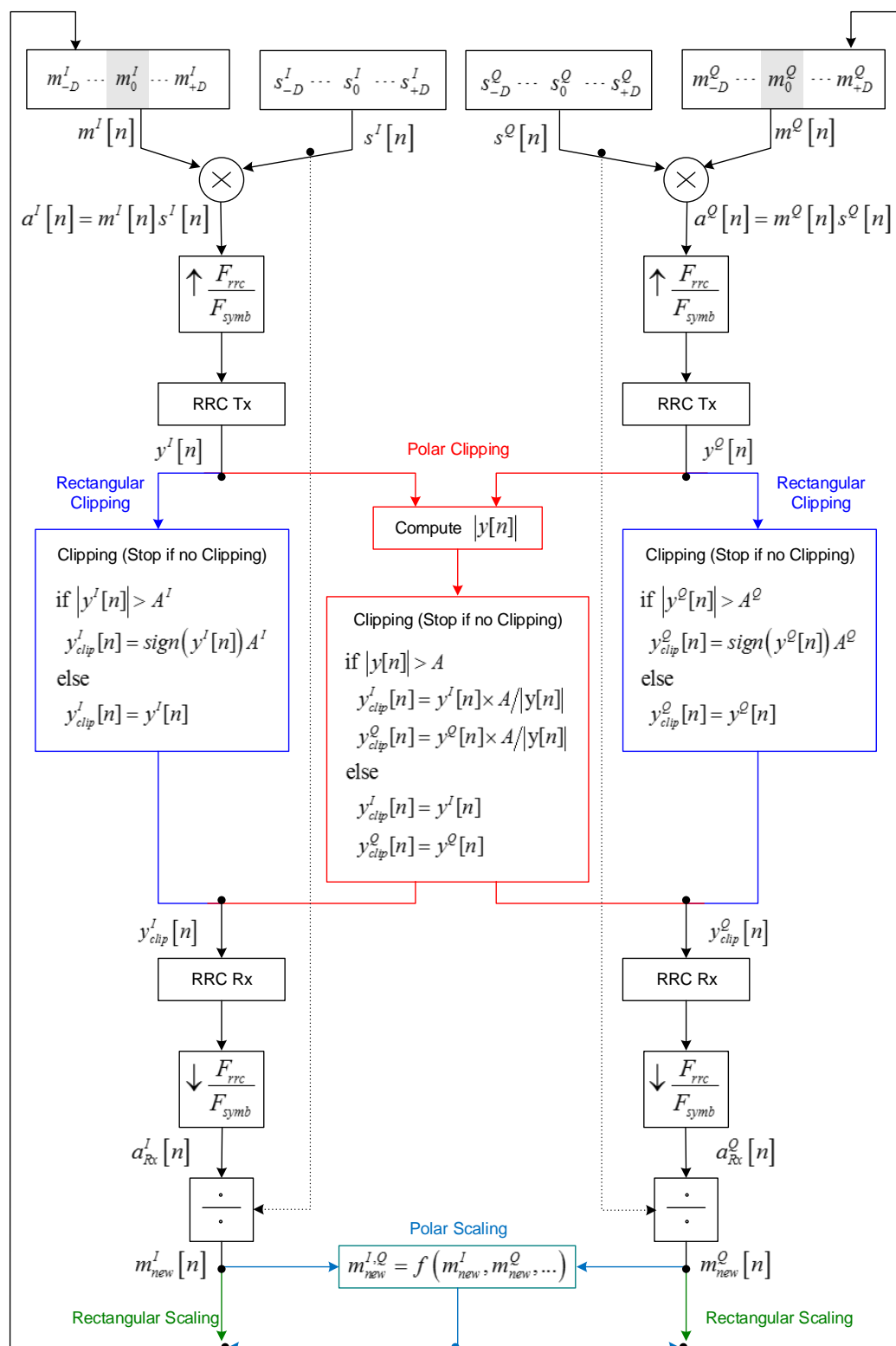
Figure 3.4: Diagram of the algorithm that computes the MM coefficients to be stored in the LUT [12].

decrease in the next iteration[6].

The number of states that a LUT needs to store depends on two factors. For a constellation with M symbols to be filtered by an RRC filter that reaches for D past and future symbols, it is needed to build a table with M^{2D+1} states. As it becomes clear, the major drawback from this fairly simple type of implementation regards the size of the constellation. Although there are some symmetries that can be explore to reduce the size of the table [12], it becomes quite impractical to design a LUT-MM method for $M \geq 16$. Concerning this issue, the work on [12] developed a robust alternative that does not require a LUT, to be described in the next subsection.

3.1.2 Multistage Polyphase Magnitude Modulation

The multistage polyphase magnitude modulation (MPMM) is a polar clipping - polar scaling MM method that is based on the implementation of the RRC filter in its equivalent polyphase representation [12, 23], as it is depicted in figure 3.5:
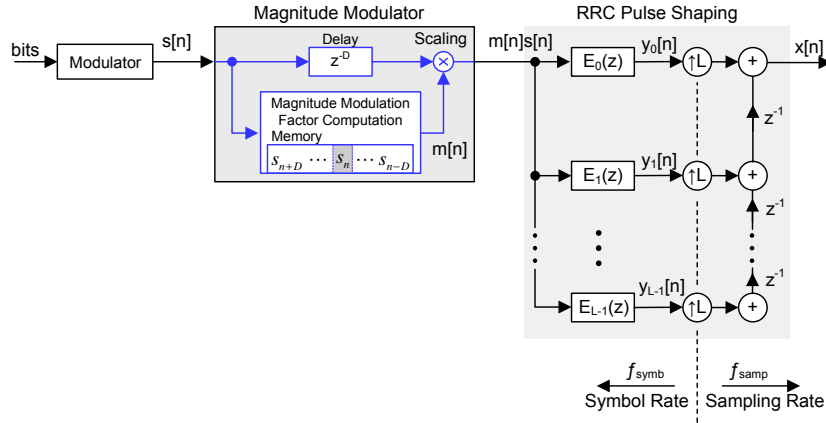
Figure 3.5: Generic Magnitude Modulation transmitter scheme, highlighting the RRC's equivalent polyphase decomposition [12, 22].

This analysis assumes, without loss of generalization, a type I linear phase FIR RRC filter whose impulse response spreads over $2N + 1$ symbols, with the transfer function $H(z)$:

$$H(z) = \sum_{n=0}^{2NL} h[n] \, z^{-n} \quad \text{with} \quad h[n] = h[2NL - n], \tag{3.3}$$

and an even oversampling factor L[7]. This polyphase decomposition enables pulse shaping filtering at symbol rate, and it is performed using the RRC components E_i as follows:

---

[6]A rough estimation of the MM may also be obtained by simply limiting the number of allowed iterations to a reasonable value.

[7]Similar developments for a type II filter [23] or an odd L can easily be inferred.
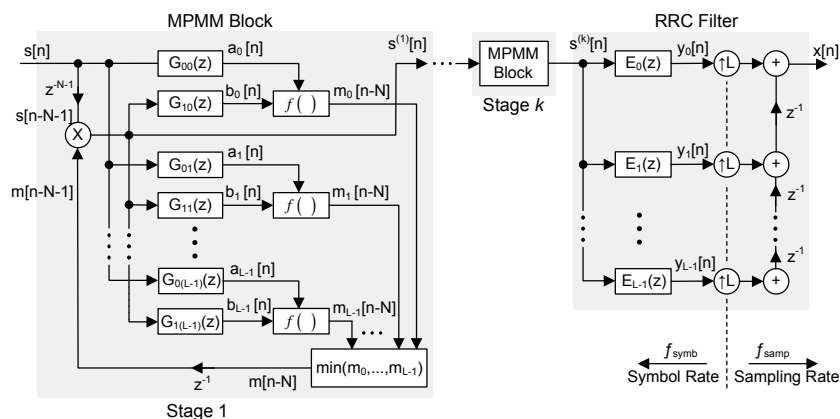
Figure 3.6: Multistage polyphase magnitude modulation scheme for controlling the signal excursion at the RRC output, followed by the RRC filter block [12, 22].

$$E_i(z) = \sum_{n=0}^{2N} e_i[n] z^{-n} = \sum_{n=0}^{2N} h[nL+i+\lambda] z^{-n} , \quad 0 \leq i \leq L-1 . \tag{3.4}$$

The parameter $\lambda \in \mathbb{Z}$ is the filter decomposition phase offset and corresponds in practice to a time-delay ($\lambda < 0$) or advance ($\lambda > 0$) of the filter impulse response. In this implementation $\lambda = -\frac{L}{2}$, in order to account for the RRC output samples where each symbol contributes the most[8].

Since RRC filtering can be described/implemented by polyphase decomposition, the RRC response prediction mentioned in section 3.1 can follow the same principle. With this in mind, figure 3.5 is upgraded to figure 3.6. All the necessary details are provided next.

The analysis of figure 3.6 starts with the filters $G_{0i}(z)$ and $G_{1i}(z)$. The RRC impulse response is divided into two parts around its center of symmetry, as shown in figure 3.7. The polyphase filters $E_i(z)$ are consequently separated into filters $G_{0i}(z)$ and $G_{1i}(z)$, respectively on the left and right, with their impulse responses given by

$$g_{0i}[n] = \begin{cases} e_i[n] & , 0 \leq n \leq N \\ 0 & , \text{ otherwise} \end{cases} , \tag{3.5}$$

$$g_{1i}[n] = \begin{cases} e_i[n+N+1] & , 0 \leq n \leq N-1 \\ 0 & , \text{ otherwise} \end{cases} . \tag{3.6}$$

This enables to separate the desired sequence in symbols that weren't evaluated and symbols that are already magnitude modulated (i.e. symbols for which its MM coefficients are already known). When MM is used, the output of $E_i(z)$ is given by (see figure 3.6)

---

[8]The work on [12] further elaborates on this topic.
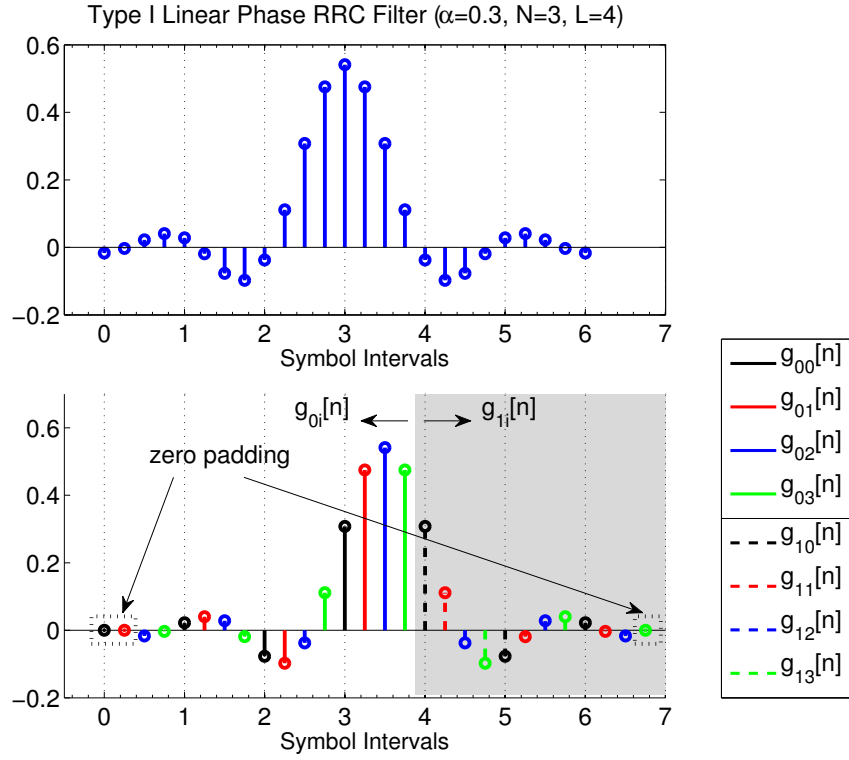
Figure 3.7: MPMM component filters, $g_{0i}[n]$ and $g_{1i}[n]$, for polyphase decomposition with phase-offset [12].

$$y_i[n] = \sum_{k=0}^{2N} e_i[k] \, m_i[n-k] \, s[n-k] \,, \quad 0 \leq i \leq L-1 \,. \tag{3.7}$$

As it was mentioned before, when computing $m_i[n_0]$, coefficients $m_i[n_0 - k]$, with $k = 1, \cdots, N$, are already known (past symbols relative to $s[n_0]$), but nothing is known about the MM values that will magnitude modulate symbols $s[n_0 - q]$ (with $q = -N, \cdots, -1$, i.e. future symbols relative to $s[n_0]$). In order to avoid excessive time variation of the average power of the signal after pulse shaping, the work on [12] assumes that future symbols should be MM as,

$$m_i[n_0 - q] \simeq m_i[n_0], \quad \text{for} \quad q = -N, \cdots, -1 \,. \tag{3.8}$$

Thus, to ensure that the envelope excursion of each RRC polyphase component's output is limited to the polar threshold A, and also considering equation (3.7) and condition (3.8), the MM factor must satisfy the condition

$$\left| m_i[n_0] \sum_{k=0}^{N} e_i[k] \, s[n_0 + N - k] + \sum_{k=N+1}^{2N} e_i[k] \, m_i[n_0 + N - k] \, s[n_0 + N - k] \right| \leq A \,, \tag{3.9}$$

and so, using definitions (3.5) and (3.6) it follows that

$$\left| \begin{array}{l} m_i[n_0] \sum_{k=0}^{N} g_{0i}[k]\, s[n_0+N-k] \\ \quad + \sum_{k=0}^{N-1} g_{1i}[k]\, m_i[n_0-k-1]\, s[n_0-k-1] \end{array} \right| \leq A \,. \tag{3.10}$$

Let $a_i[n]$ and $b_i[n]$ denote the complex signals at the output of filters $G_{0i}(z)$ and $G_{1i}(z)$ as shown in figure 3.6. Examining (3.10) and considering the convolution's definition, it is straightforward to conclude that

$$\sum_{k=0}^{N} g_{0i}[k]\, s[n_0+N-k] = a_i[n_0+N] \,, \tag{3.11}$$

and,

$$\sum_{k=0}^{N-1} g_{1i}[k]\, m_i[n_0-k-1]\, s[n_0-k-1] = b_i[n_0+N] \,. \tag{3.12}$$

As a result, condition (3.10) can be expressed as

$$|m_i[n_0]\, a_i[n_0+N] + b_i[n_0+N]| \leq A \,. \tag{3.13}$$

In order to guarantee condition (3.13), a non-negative $f(\cdot)$ was defined by [12] to compute $m_i[n_0]$:

$$m_i[n_0] = f_{\mathsf{MM}}(A, a_i[n_0+N], b_i[n_0+N]) \,, \tag{3.14}$$

where

$$f(A,a,b) = \begin{cases} 1 & ,|a+b| \leq A \\ \dfrac{-Re\{ab^*\} + \sqrt{Re\{ab^*\}^2 - |a|^2(|b|^2 - A^2)}}{|a|^2} & ,|a+b| > A \end{cases} \,, \tag{3.15}$$

for $A \in \mathbb{R}^+$ and $a,\, b \in \mathbb{C}$. This analysis is further extended in [12]. Since the output of all filters $E_i(z)$ must satisfy condition (3.13), the symbol to be magnitude modulated is multiplied by the most restricted factor, i.e.

$$m[n] = \min_{i=0,\cdots,L-1} (m_i[n]) \,. \tag{3.16}$$

When computing the MM coefficient with (3.15), condition (3.8) is assumed to be true, which may not be the case. Although condition (3.13) is satisfied even when the coefficient $m[n_0+1]$ is smaller than $m[n_0]$, this does not happen when $m[n_0+1] > m[n_0]$. A simple procedure that guarantees that the condition (3.13) is only slightly violated on those occasions was found by using the time variant filter [12, 22]:

$$m[n+1] > m[n] \;\Rightarrow\; m'[n+1] = \frac{m[n+1]+m[n]}{2} \tag{3.17}$$

This MPMM procedure is fairly simple and it is scalable for constellations with $M \geq$ 16 symbols, with considerable net back-off gain[9] [12], surpassing the LUT method as the MM state of the art procedure.

3.1.3 Magnitude Modulation for OQPSK signals

When designing an equivalent MM scheme for OQPSK some questions arise. The OQPSK signal's envelope has fewer excursions than an equivalent QPSK signal[10] (see figure A.4, in appendix A), which is a consequence from offsetting its in-phase and quadrature signal components. This results in a necessarily lower PAPR signal, thus reducing the potential gain margin that could be obtained by employing MPMM instead of LUT-MM.

Besides, to deal with the time offset between the two signal components it makes more sense to use a rectangular scaling approach, making the number of required assumptions escalate (the assumptions to be made would need to account both component coefficients, which is not as straightforward as condition (3.8) in the MPMM case).

Alternatively, Tomlinson's LUT method could be applied to an OQPSK signal to address the LINC requirements (namely a high oversampling rate), and the PAPR of the resulting magnitude modulated signals are shown in figure 3.8. The simulations carried along this chapter use an RRC filter with a 25% roll-off factor (spreading over 7 past and future symbols) and an oversampling factor $L = 8$.

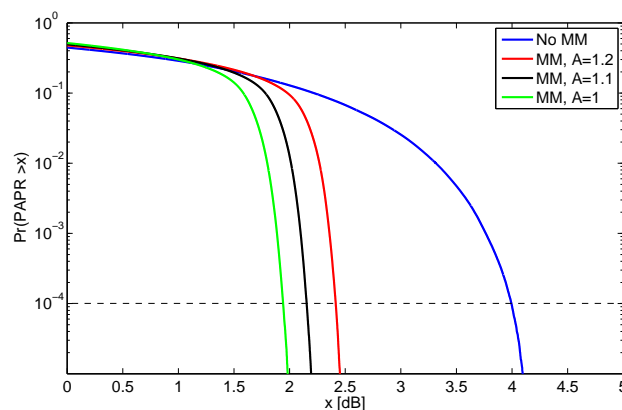Figure 3.8: Comparison of the PAPR of the magnitude modulated OQPSK signals (using the LUT method) with the equivalent OQPSK signal without MM.

---

[9]This measurement accounts for the back-off gain in the transmitter and the distortion losses at the receiver for a given BER level.

[10]All considerations are made regarding QPSK and OQPSK signal's with the same average power, for a fair comparison.

Although this MM scheme successfully reduces the PAPR of the OQPSK signal (over 2dB PAPR gains at a probability of 10^{-4} for the MM threshold $A = 1$), this reduction is not enough to satisfy the LINC oversampling requirements. As figure 3.9 shows, the spectrum of the LINC signal components is negligibly reduced, even though stringent limits were enforced by the MM thresholds.
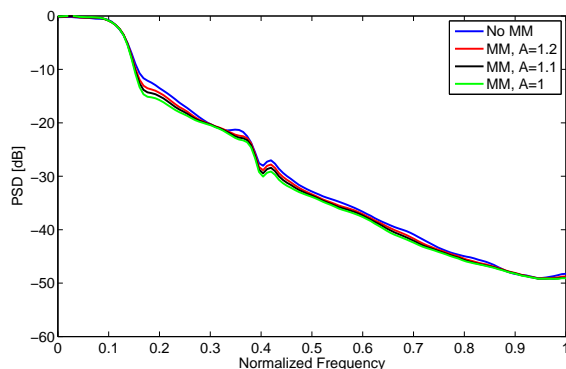
Figure 3.9: PSD of one of the LINC branches s_{n1}, for different LUT-MM boundaries sets.

This result is related to the transition path diagram of the magnitude modulated signals, like the one illustrated in figure 3.10. This figure shows that limiting the envelope excursions to an upper bound also scales down the inner most samples (as expected), which results in a broader decomposition angle θ range (see equation (2.7)), which in turn broadens the spectrum of the LINC components s_{n1} and s_{n2} (see equations (2.3) and (2.4)).
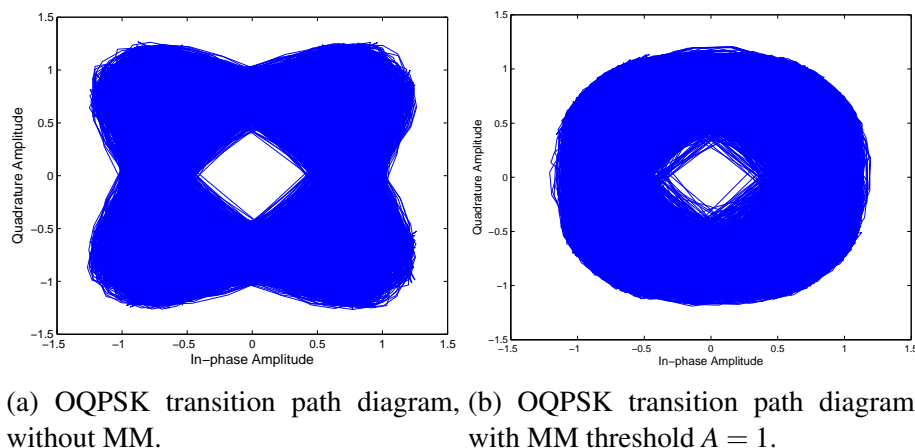
(a) OQPSK transition path diagram, without MM.

(b) OQPSK transition path diagram, with MM threshold $A = 1$.

Figure 3.10: Diagram of the transition path between the constellation's symbols of a magnitude modulated OQPSK signal, comparing the case where it is used a LUT method with MM threshold $A = 1$ with an OQPSK signal where MM was not applied.

Considering the LINC combiner's concerns regarding the decomposition angle θ (see figure 2.4 in subsection 2.2.2) and the LINC oversampling requirements, the next section

presents a new MM approach to fit these constraints.

3.2 Ring-type Magnitude Modulation on OQPSK signals

The existing MM procedures only address the signal's envelope maximum excursions, since they are usually applied to SC transmission schemes that employ linear HPAs, which face the previously mentioned PAPR problem [4, 8]. However, by making the use of LINC techniques, energy efficiency of the front-end amplification module is mainly limited by the combiner's efficiency [6, 9]. By observing figure 2.4 one could infer that higher combiner's energy efficiency can be achieved by also reducing the higher phase content of the decomposition angle[11] θ, i.e. by also enforcing a lower bound on the LINC input signal's amplitude (see equation (2.10), regarding instant combiner's energy efficiency).

Considering this, the OQPSK modulation scheme, that avoids simultaneous passages through zero of the in-phase and quadrature signal's components, seems to fit better the LINC requirements for higher efficiency, since its envelope has smaller variations than the equivalent QPSK signal (see figures A.3 and A.4 in appendix A). Nonetheless, bandwidth pulse shaping of OQPSK signals still introduces some envelope variations. The development of ring-type MM techniques able to perform simultaneous upper and lower amplitude limitation would be desirable.

The following subsections further explain the proposed ring-type magnitude modulation (RMM) scheme.

3.2.1 Ring-type Magnitude Modulation Algorithm

In this approach, it is explored the amplitude properties of the OQPSK modulation scheme in the development of a new RMM method that fits the LINC transmission system's requirements. Considering the obstacles imposed by this type of modulation for a MPMM type of approach, this scheme makes use of a look-up table to store all possible states, i.e. all the MM coefficients are computed *a priori* and stored in the LUT.

Since there is a time offset between the in-phase and quadrature signal components (the implications are discussed in appendix A), each component has a different scaling factor, to provide a finer control of the signal envelope. Besides, this method enforces upper and lower polar boundaries on the magnitude modulated signal, making this a polar clipping-rectangular scaling type of method.

Figure 3.11 illustrates the MM coefficients computation process of the proposed scheme[12].

---

[11]Instead of simply reducing the signal's PAPR.

[12]This explanation is briefer than the one in section 3.1.1, because the same reasoning applies to this method. As previously, this analysis follows the diagram's notation.

Before performing the polar clipping operation, the time offset of the signal components is taken into account in a similar way to the one depicted in figure A.2 (see appendix A). As previously stated, the signal clipping operation performed in this scheme has two amplitude thresholds: the lower boundary A_l and the upper boundary A_u. Therefore, each iteration evaluates if the following condition is satisfied:

$$A_l \leq |y[n]| \leq A_u \,, \tag{3.18}$$

properly rescaling the samples that fall outside these limits. Once again, the MM coefficients are obtained by dividing the received signal components $a_{Rx}^I[n]$ and $a_{Rx}^Q[n]$ by the original sequences $a^I[n]$ and $a^Q[n]$, respectively (like in Tomlinson's RS method [11], and accounting for the time offset between the in-phase and quadrature components on the sampling process). The discussion about the LUT approach in subsection 3.1.1 also applies for the proposed scheme.

Each MM coefficient significantly affects L samples (as stated in subsection 3.1.2), and when the upper and lower boundaries become more stringent there are situations when the envelope of the mentioned sequence crosses both boundaries (see figure 3.12). However, this challenge is overcome because the RMM coefficients calculation accounts for a sequence of $2D + 1$ symbols (as depicted in figure 3.3), instead of considering only the affected symbol, like in the MPMM method.

After describing the RMM coefficients computation, the next step of this work is to define the amplitude boundaries A_l and A_u, as presented in the next subsection.

3.2.2 Choosing the RMM parameters

This subsection's main focus is to define the proposed RMM method's boundaries A_l and A_u, namely regarding the LINC combiner's requirements for high energy efficiency. For clarity, this boundaries are defined assuming that the signal to be magnitude modulated has unitary average power[13]. Therefore, besides the BER performances (that assess the effect of the MM added distortion on signal transmission) and the diagrams of the transition paths between the constellation's symbols (that illustrate the MM procedure), each boundary set evaluation includes an estimation of the probability density function (PDF) of the decomposition angle θ of the magnitude modulated signals (using equation (2.7)), in order to find the best MM configuration to include in the proposed transmission system.

There are two possible ways of obtaining the information necessary to make a reasoned choice of the MM polar boundaries: the cumulative distribution function (CDF) of

---

[13]This analysis is valid for a generic average power σ^2, with equivalent upper and lower boundaries $\frac{A_u}{\sigma}$ and $\frac{A_l}{\sigma}$, respectively.
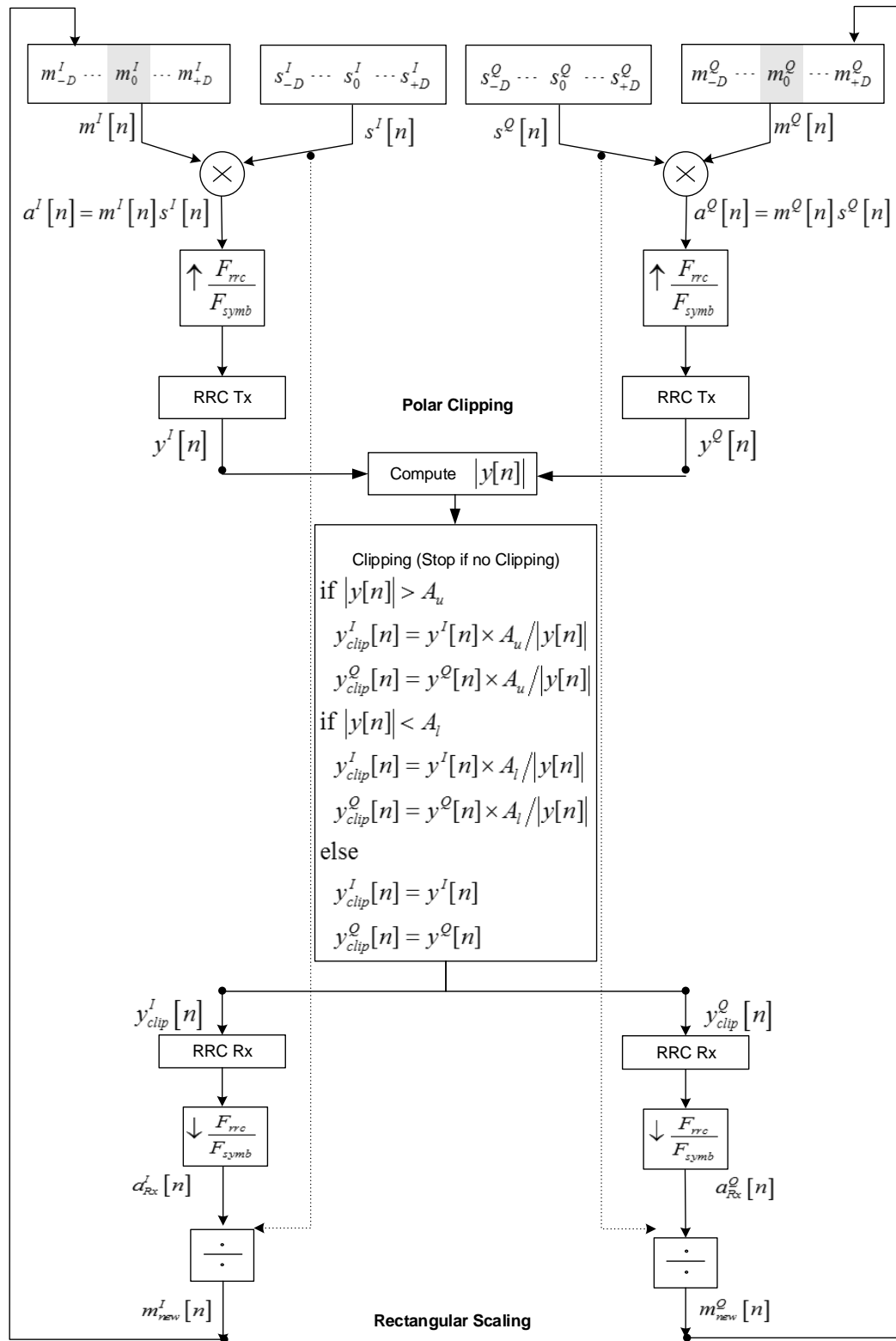
Figure 3.11: Diagram of the new algorithm that computes the MM coefficients to be stored in the LUT.
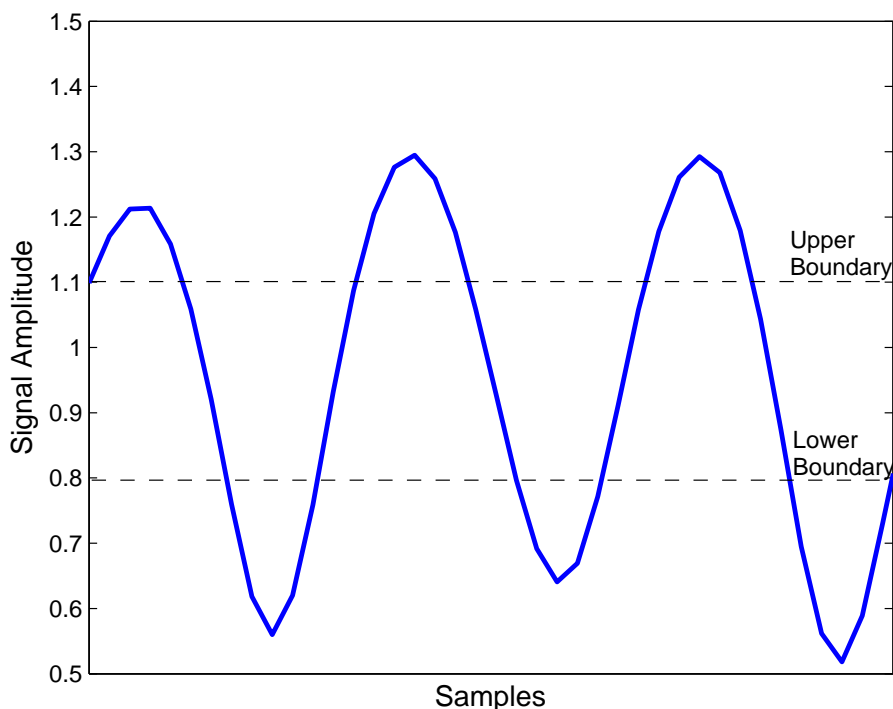
Figure 3.12: Samples corresponding to a sequence of five random symbols (without MM), to be limited by $A_l = 0.8$ and $A_u = 1.1$. The sequence where those samples where extracted has unitary average power.

the OQPSK signal amplitude and the PDF of the corresponding decomposition angle θ. Since the LINC signal separator enforces polar clipping, the first option seems to be more practical[14].

Accordingly, figure 3.13 represents the amplitude CDF of an RRC filtered OQPSK signal, with an oversampling factor $L = 8$ (see subsection 2.2.1). The proposed scheme's RRC filter has a 25% roll-off factor, as it is used in typical communication systems [24]. However, since the pulse shaping filter is the main source of envelope variations on the filtered signal (due to the 0dB contribution of the OQPSK constellation to the PAPR [12, 22]), designing an RMM method with a different roll-off factor requires a similar study of the amplitude of the filtered OQPSK signal as the one that is done in this work.

The analysis of figure 3.13 reveals that setting the lower boundary A_l to 0.7, 0.8 and 0.9 would imply scaling up at least 10%, 25% and 40% of the signal's samples, respectively. Likewise, setting the upper boundary A_u to 1.3, 1.2 and 1.1 would involve scaling down, respectively, 10%, 20% and 30% of the signal's samples. With this in mind, figure 3.14 shows the transition path diagrams of OQPSK signals where the proposed RMM

---

[14]The alternative is using equation (2.7) to associate each angle θ with its corresponding amplitude level, which makes the notation and the analysis needlessly more obscure.
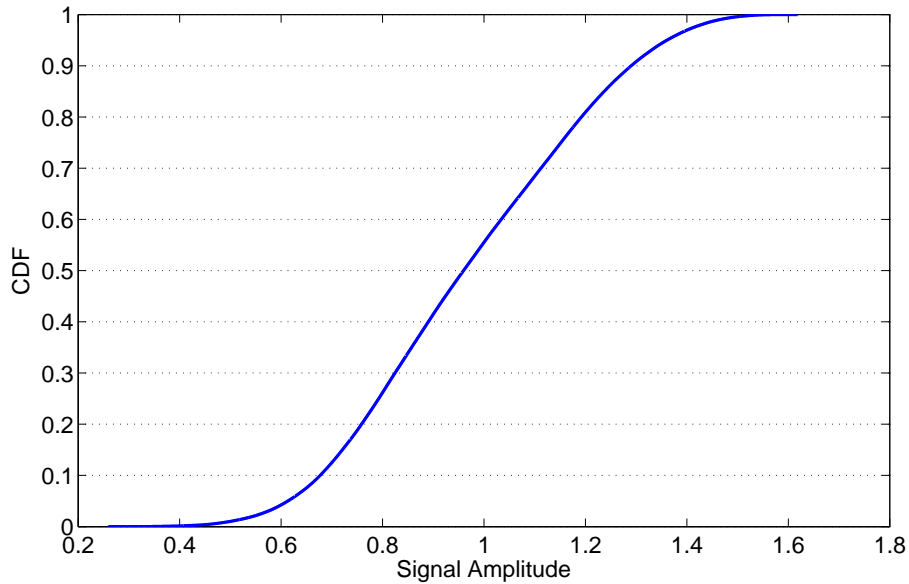
Figure 3.13: CDF of an OQPSK RRC filtered signal (without MM).

scheme was applied, using the mentioned boundaries[15].

The rest of this chapter uses these sets of RMM boundaries, either if this procedure is applied to generic SC transmitter schemes that employ linear HPAs or in the LINC context (as it is proposed in this work).

3.3 Performance Evaluation of the Ring-type Magnitude Modulation

This section reports the gains obtained when the proposed RMM method is applied on two distinct SC scenarios. The first subsection addresses the case where a linear HPA is employed, while the second subsection evaluates the impact of the RMM method on a LINC transmitter scheme.

3.3.1 RMM parameters for transmitters employing linear HPAs

Typical methods that control the transmitted signal's envelope excursions are developed to be included in transmitter schemes that work with linear HPAs (like the one depicted in figure 3.1), aiming to reduce the PAPR of the band limited transmitted signal and the required back-off to drive the linear HPA close to saturation [1, 11, 12]. Accordingly, this subsection briefly reports gains obtained when the proposed RMM method is used on such transmitter schemes.

---

[15]These transition path diagrams should be compared with the original signal's, depicted in figure A.3b.

(a) Set #1: $A_l = 0.7$ and $A_u = 1.3$.

(b) Set #2: $A_l = 0.9$ and $A_u = 1.3$.

(c) Set #3: $A_l = 0.8$ and $A_u = 1.2$.
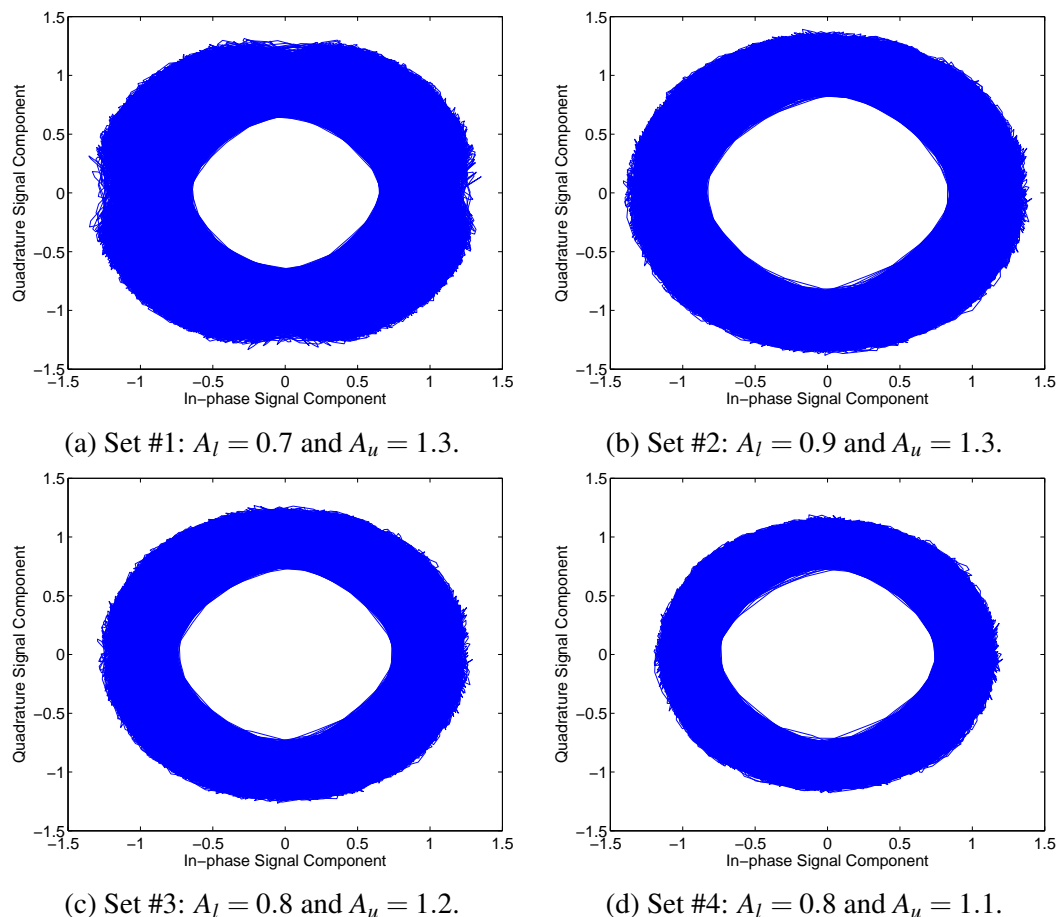
(d) Set #4: $A_l = 0.8$ and $A_u = 1.1$.

Figure 3.14: Magnitude modulated OQPSK signals with different sets of upper and lower boundaries. These signals had unitary average power before MM was employed, in order to illustrate the MM boundaries' effect.

Figure 3.15 depicts the PAPR of the magnitude modulated signals represented in figure 3.14. As it is shown, the MM amplitude constraints imposed on the OQPSK signals result in PAPR reduction gains of at least 1dB for probability of 10^{-4} (the reference is a system without MM). However, this analysis needs to be complemented with the BER performance of the transmission system, in order to account for the MM distortion loss on the net gain. Those losses are depicted in figure 3.16, where it is evaluated the system's performance over an additive white gaussian noise (AWGN) channel for different $Eb/N0$ values[16]. In these simulations it is used channel error control coding relying on an low-density parity-check (LDPC) (1680,840) code [25].

---

[16]$Eb/N0$ represents the energy per bit to noise power spectral density ratio.
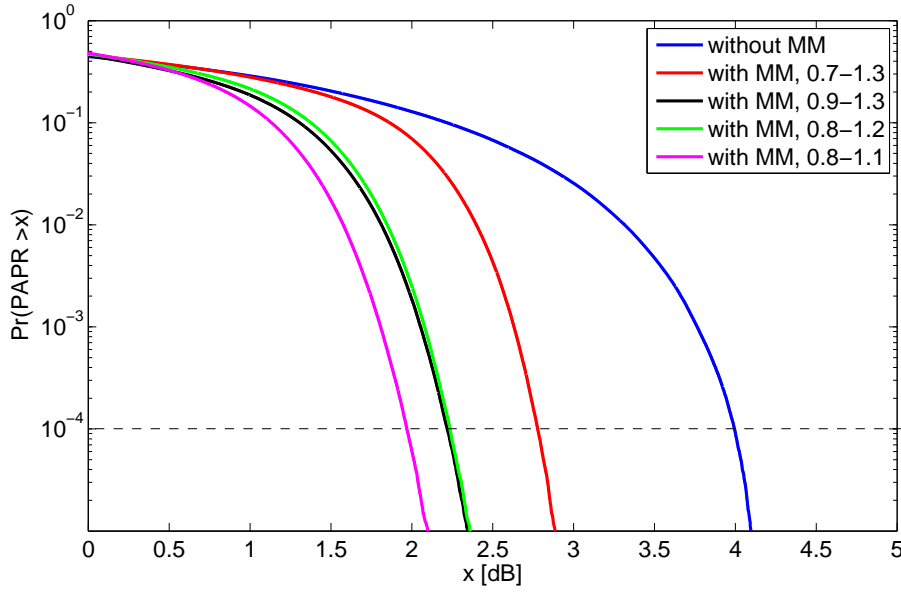
Figure 3.15: Comparison of the PAPR of the RMM OQPSK signals show in figure 3.14 with an OQPSK signal that is not magnitude modulated.

The analysis of figures 3.15 and 3.16 leads to table 3.1, where it is summarized the systems' net back-off gain. This measure is estimated as follows:

$$Gain = (PAPR_{NoMM} - PAPR_{MM}) - [Eb/N0_{MM}(@BER) - Eb/N0_{NoMM}(@BER)] .$$

$$(3.19)$$

Table 3.1: Table with the net back-off gain at $BER = 10^{-4}$ provided by the proposed RMM scheme.

Set	$PAPR@10^{-4}$	$Eb/N0@BER = 10^{-4}$	Net back-off gain
No MM	3.995 dB	1.805 dB	–
#1	2.779 dB	2.043 dB	0.978 dB
#2	2.219 dB	2.657 dB	0.924 dB
#3	2.236 dB	2.526 dB	1.038 dB
#4	1.969 dB	2.931 dB	0.900 dB

The results in table 3.1 show that using the MM boundaries set #3 ($A_l = 0.8$ and $A_u = 1.2$) provide this method's best outcome for typical SC transmitter schemes that employ linear HPAs, with 1dB net back-off gain. A transmission system using a magnitude modulated OQPSK signal in such conditions can be a reasonable alternative to the QPSK's MPMM method, since this constellations avoids all zero-crossings and it has a fairly low PAPR of 2.236dB (see table 3.1).
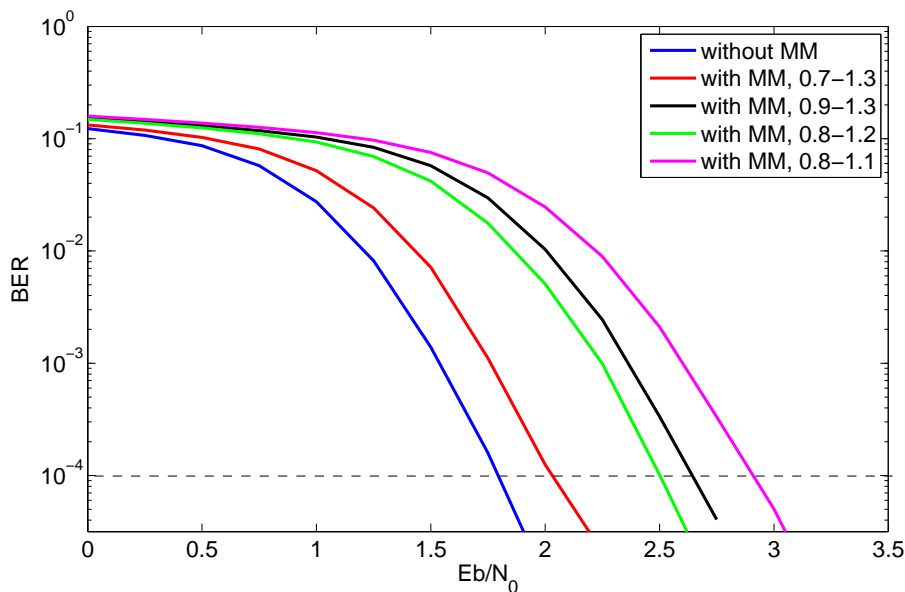
Figure 3.16: BER performance of LDPC-coded magnitude modulated signals in figure 3.14 and the original signal, in a generic SC transmission scheme and over an AWGN channel.

After this developing regarding a generic SC transmitter scheme that employs linear HPAs, this work proceeds to the next subsection where the proposed RMM method is explored to achieve the LINC transmission system's potential efficiency.

3.3.2   RMM Parameters on the LINC context

Since the goal of the proposed RMM scheme is to be included in a LINC transmission system, this subsection starts with a more suited evaluation of this scheme, that attends the challenges described in subsection 2.2.2. Figure 3.17 illustrates how the decomposition angle θ spreads over a smaller range on OQPSK signals where RMM is employed. All of these simulations have the same LINC amplitude clipping threshold, which was set to be adequately high so that none of the OQPSK signals would suffer distortion from it.

Although an empirical evaluation about the LINC combiner's energy efficiency can be made by observing figure 3.17 (an intuitive guess associates higher combiner's efficiency with a smaller range of possible decomposition angles), it is critical to use equation (2.11) from subsection 2.2.2 to make an informed choice between the different sets of boundaries. Thus, table 3.2 contains the necessary information to evaluate each set of MM boundaries. As it was mentioned, the clipping level s_M is a critical factor in the LINC's combining efficiency. Therefore, each efficiency value was estimated assuming that only 0.01% of the samples were clipped, which is an acceptable approximation of an unclipped signal (in terms of spectral regrowth outside the transmitted signal's frequency band).
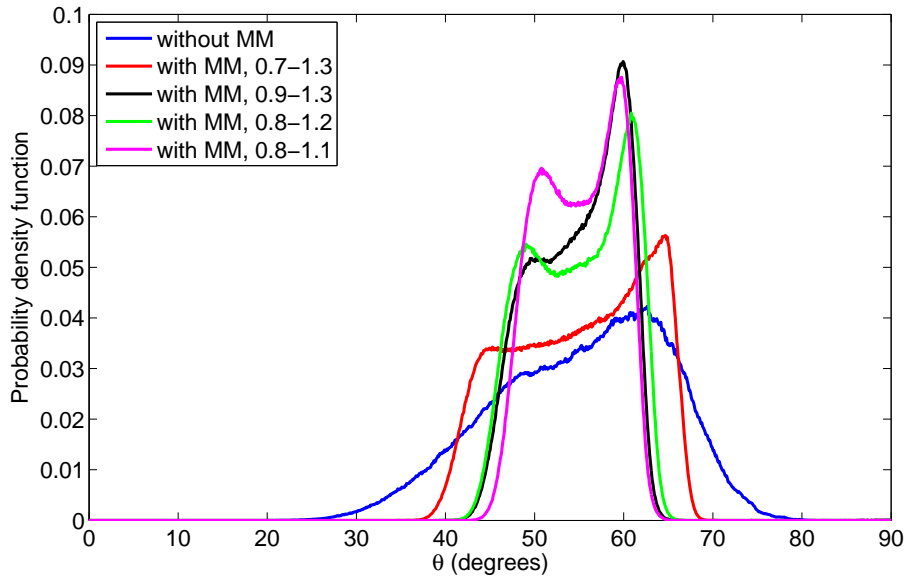
Figure 3.17: Distribution of the decomposition angle of the magnitude modulated signals in figure 3.14, compared with the original signal.

Table 3.2: Table of the LINC combiner's energy efficiency $\overline{\eta}_{comb}$ when a magnitude modulated OQPSK signal is transmitted.

Set	$\overline{\eta}_{comb}$	**PAPR** @10^{-4}	$Eb/N0$ @**BER**
No MM	39.9%	3.995 dB	1.805 dB
#1	52.7%	2.779 dB	2.043 dB
#2	60.0%	2.219 dB	2.657 dB
#3	59.8%	2.236 dB	2.526 dB
#4	63.5%	1.969 dB	2.931 dB

The results show that by simply including the proposed RMM scheme with the most flexible boundaries set tested ($A_l = 0.7$ and $A_u = 1.3$), the LINC combiner's average efficiency can be improved by 13% with negligible BER performance loss. The best outcome comes from enforcing the boundaries set #4 ($A_l = 0.8$ and $A_u = 1.1$), for which the combining efficiency rises to 63.5% (a nearly 25% upgrade over the scheme that did not employ RMM), reporting only 1.1dB loss for BER $= 10^{-4}$.

Regarding the LINC's oversampling requirements, figure 3.18 presents the PSD of one of the LINC branches. As it was expected, the reduced PAPR signals obtained by MM the original OQPSK signal results in a smaller spectrum spreading, thus effectively reducing the necessary bandwidth to be accommodated by the HPAs. Like in the previous situation, the best outcome is provided by set #4.

In the next chapter it will be studied the implementation of the developed RMM
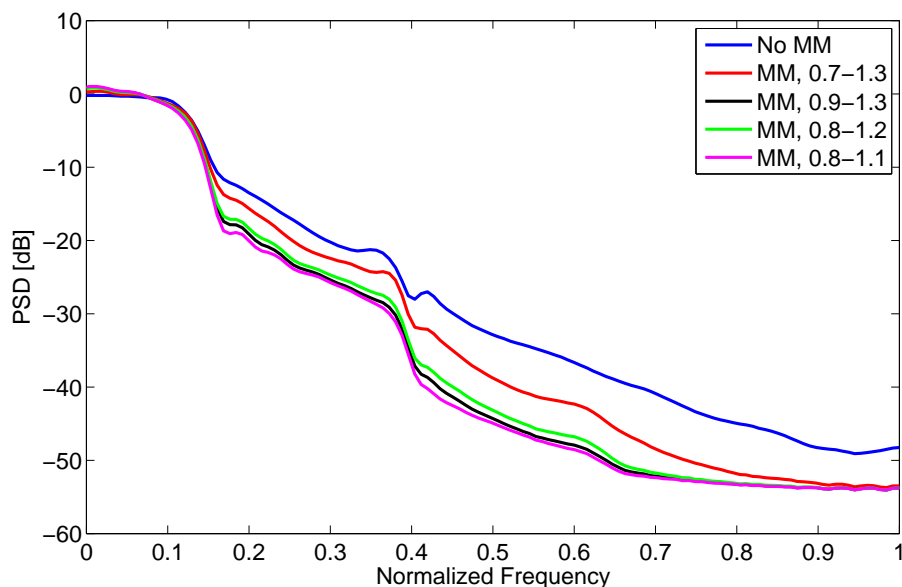
Figure 3.18: PSD of one of the LINC branches s_{n1}, for different RMM boundaries sets.

scheme on a LINC transmission scheme using the set of boundaries #4, considering the different challenges faced by this type of transmitters (as described in chapter 2). Also, it will be inspected if further efficiency improvements can be achieved on this already efficient magnitude modulated LINC transmitter, by exploring the possible tradeoffs that allow higher energy efficiency (resulting from additionally performing polar clipping at the LINC separator block) at the expense of negligible spectral regrowth outside of the signal's frequency band[17].

---

[17]As it was mentioned before, post-filtering clipping operations may result in spectral spreading, causing loss of bandwidth efficiency and undesirable adjacent channel interference [12].

4

Magnitude Modulated LINC transmission system

Contents

Chapter 2 discussed the close relation between the LINC clipping level s_M and its combiner's energy efficiency, stating that lowering the polar threshold would result in enhancing energy efficiency at the expense of increase the transmitted signal's bandwidth, due to the spectral spreading caused by post-filtering clipping. However, a small amount of distortion can be endured, and that is why this chapter focuses on evaluating the effect of the threshold level s_M on the proposed magnitude modulated LINC transmission system.

The first section describes the proposed combined ring-type magnitude modulation with LINC transmitter scheme, and the experiments that were performed. The simulation results of this scheme are presented in section 4.2, regarding the BER performance, the spectral spreading of the transmitted signal and the LINC requirements (oversampling and combiner's efficiency). After choosing an adequate LINC clipping level s_M, the third subsection evaluates the overall system when there are gain and phase imbalances between the HPAs.

4.1   Magnitude Modulated LINC transmitter scheme

Figure 4.1 illustrates the proposed transmitter scheme. The simulations carried along this chapter use an OQPSK digital modulator, an RRC filter with a 25% roll-off factor (spreading over 7 past and future symbols), an oversampling factor $L = 8$, and MM set of boundaries $\{A_l = 0.8, A_u = 1.1\}$. Like in the previous chapter, these simulations used channel error control coding relying on an LDPC (1680,840) code [25].
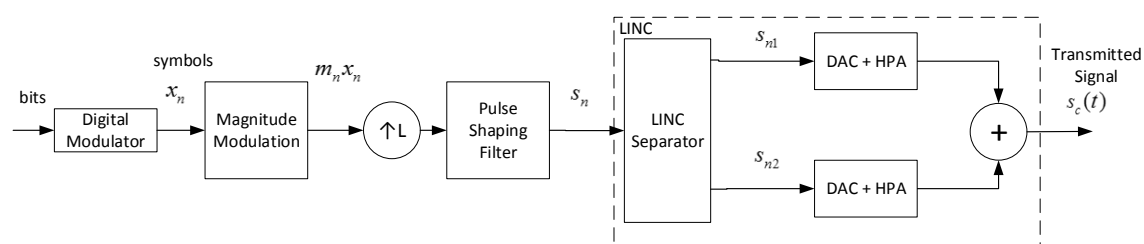
Figure 4.1: Magnitude modulated LINC transmission scheme.

Before explaining the s_M selection process, it should be emphasized that the signal fed to the LINC s_n is scaled to ensure that the signal has average unitary power, which means that the inner and outer bounds A_l and A_u are scaled versions of the ones set in chapter 3. It should also be noted that the analysis done in this chapter is equally valid if s_n has σ^2 average power, by replacing the LINC clipping level s_M for an equivalent clipping ratio s_M/σ.

Figure 4.2 represents the amplitude CDF of the RMM OQPSK signal. In order to

ensure a controlled amount of spectral regrowth on the transmitted signal s_c, these experiments' clipping levels s_M ranges between 1 and 1.2.
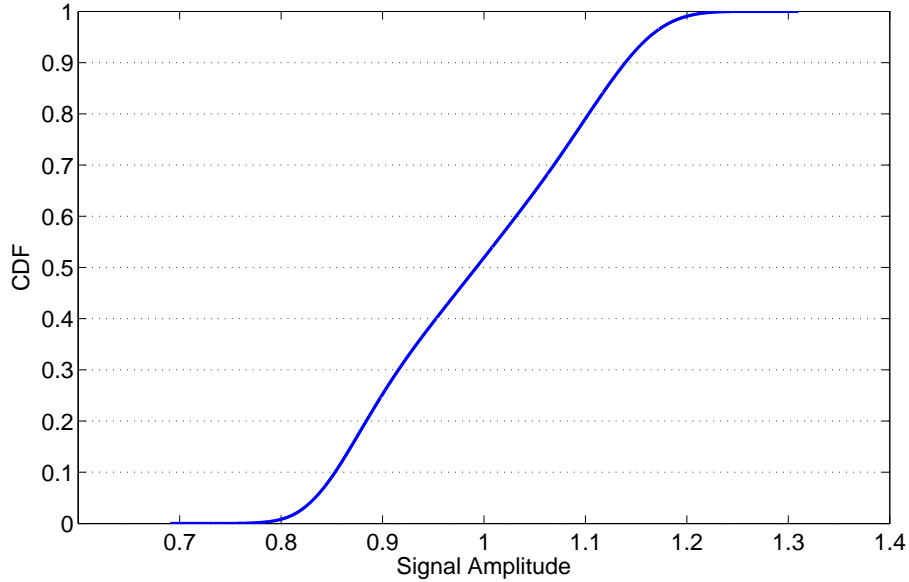
Figure 4.2: Amplitude CDF of the Magnitude Modulated OQPSK signal.

4.2 Simulation results

As it was mentioned before, this section reports the results regarding the implementation of the proposed combined ring-type magnitude modulation with LINC transmitter scheme and the effect of the LINC clipping threshold on the overall performance of the transmitter.

4.2.1 BER performance

Figure 4.3 presents the BER performance for RMM combined with the LINC technique on OQPSK signals, employing LDPC coding. As it shows, the studied clipping thresholds s_M induced performance losses are negligible when compared to the unclipped ring-type magnitude modulation case.

Figure 4.3: BER performance of the magnitude modulated LINC transmitter for different clipping levels s_M.

4.2.2 LINC oversampling requirements' analysis
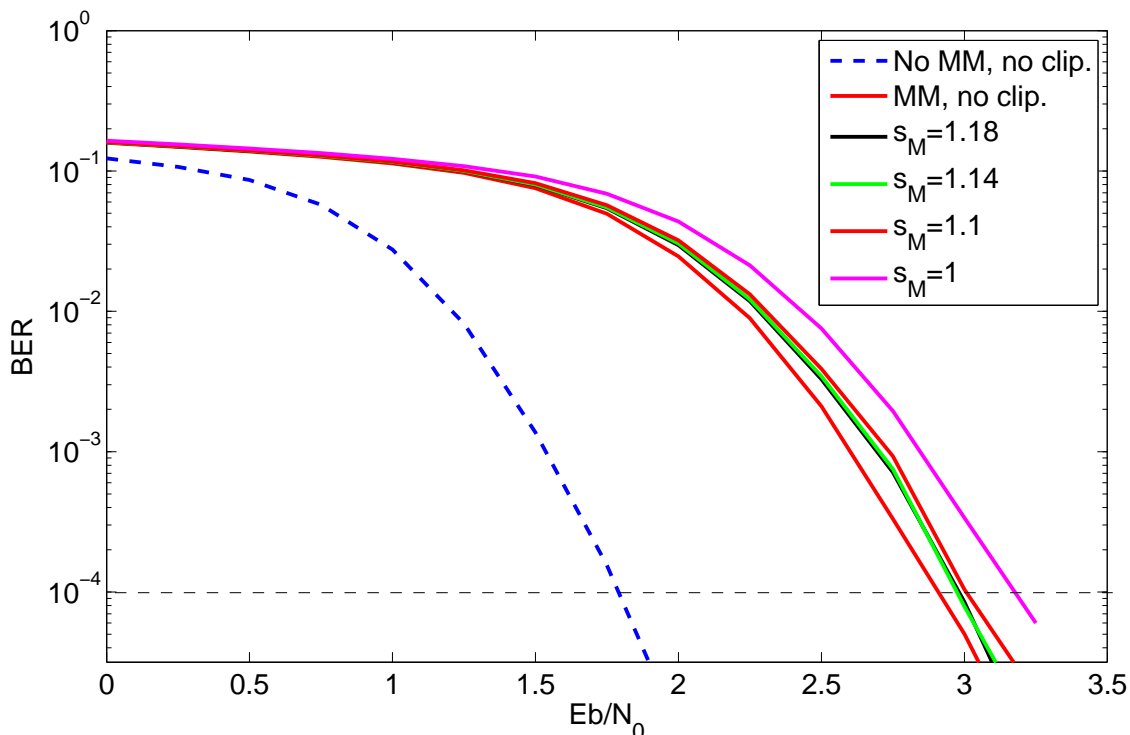
Figure 4.4 presents the PSD of one the LINC branches s_{n1} (since both branches have equal power spectra, as mentioned in subsection 2.2.1) for different clipping levels s_M. As it was mentioned before, performing RMM on the OQPSK signal reduces the spectral enlargement of the LINC signal components s_{n1} and s_{n2}, which means that the NL HPAs employed need to accommodate a smaller bandwidth when comparing to the unmodulated OQPSK signal. The increased attenuation achieved is related to the reduced phase modulation on the LINC branches (see subsection 2.2.1), as a result of keeping the decomposition angle on a smaller range.

Although each of the illustrated cases have a similar PSD's lower frequency band, the post-filtering clipping procedures (when applicable) induce spectral regrowth beyond the mentioned frequency band. As expected, this spectral regrowth increases as the clipping level s_M decreases. Accordingly, the LINC clipping level to be chosen should not be smaller than 1.1, below which s_{n1}'s PSD does not flatten beneath $-40dB$ for $f \geq 0.4$.
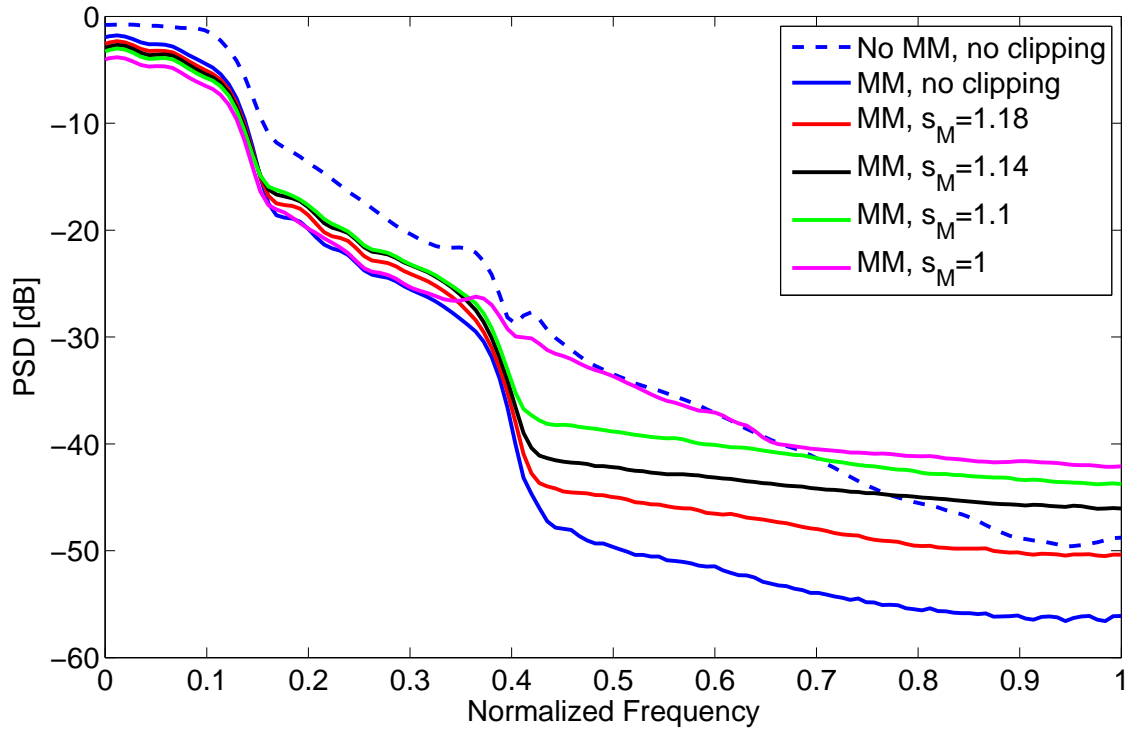
Figure 4.4: PSD of one of the LINC branches s_{n1}.

4.2.3   System's spectral efficiency

The reconstructed signal s_c's PSD is shown in figure 4.5, where it is once again depicted the spectral spreading caused by successively lowering the clipping threshold s_M. It can be also be noted that the proposed RMM scheme (like its equivalent procedures) does not increase the transmitted signal's bandwidth, since the distortion is performed before RRC filtering the symbol sequence x_n.

Like in the previous subsection's analysis, the LINC clipping level to be chosen should not be smaller than 1.1, since s_c's PSD stopband attenuation significantly decreases below this level.
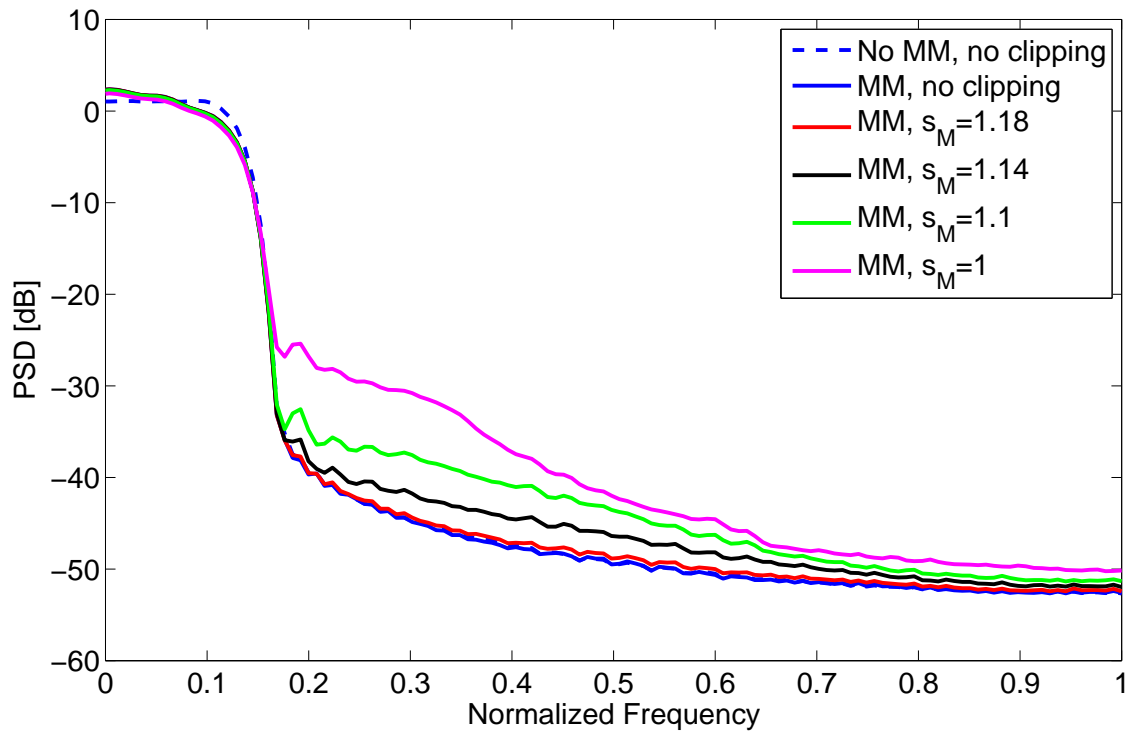
Figure 4.5: PSD of the reconstructed signal s_c.

4.2.4 LINC combiner's average energy efficiency

Figure 4.6 shows how the distribution of the decomposition angle θ varies with the LINC clipping level s_M. A simple inspection on equations (2.7) and (2.10) is enough to conclude that the clipped samples accumulate on the angle $\theta = 0°$ (hence the impulse[1] on the PDF at that decomposition angle), and are combined with 100% energy efficiency. This is why the lower clipping threshold LINC transmitters achieve higher combiner's energy efficiency, has it is shown in table 4.1.

Table 4.1: LINC combiner's efficiency, for the studied scenarios.

s_M/σ	No Clip.	1.2	1.18	1.16	1.14	1.12	1.1	1
$\overline{\eta}_{comb}$	63.5%	69.4%	71.7%	74.1%	76.5%	78.8%	81.0%	90.7%

---

[1]These impulses are not to scale, and instead they should be compared by using their respective area.

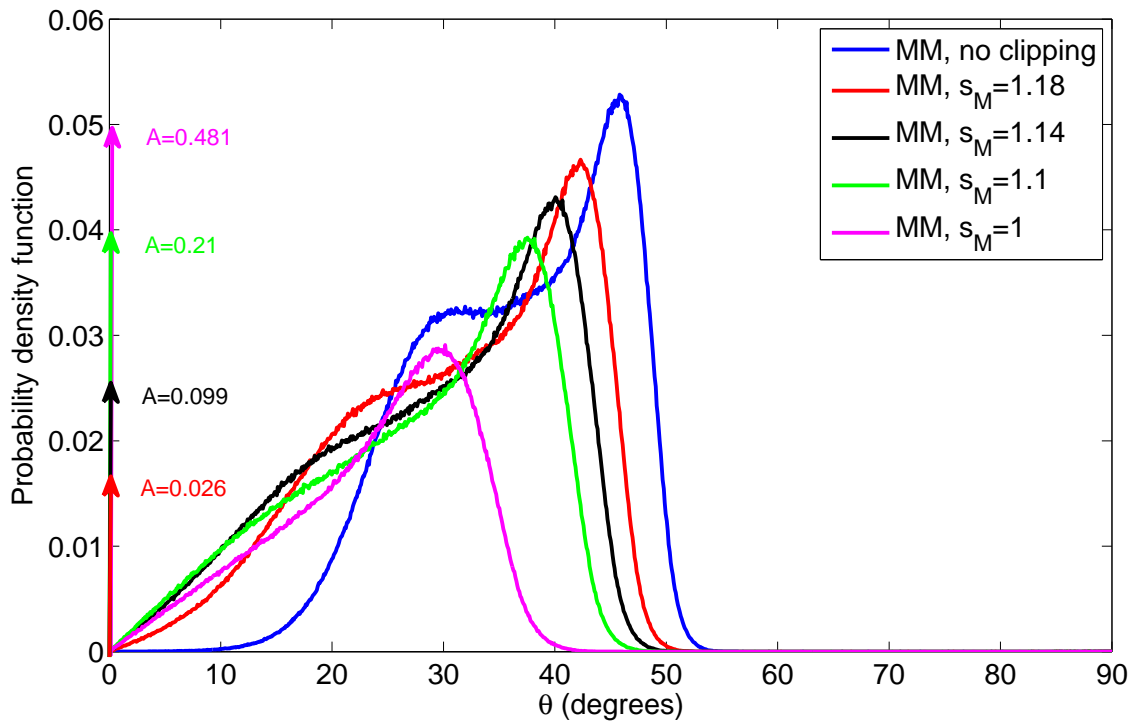Figure 4.6: Distribution of the decomposition angle of the ring-type magnitude modulated signal fed to the LINC separator block. Each clipped scenario has an impulse on the PDF at $\theta = 0$, and the respective area is written in the same color as the corresponding scenario.

4.2.5 Choosing the clipping level s_M

After this section's analysis and discussion, it is chosen the clipping level $s_M = 1.14$, as it is a good compromise between the combiner's energy efficiency and the allowed signal distortion, namely regarding the LINC oversampling requirements and the transmitted signal's spectral regrowth. In the next section it will be studied the impact of gain and phase imbalances between the LINC's HPAs.

4.3 Amplification Imbalances

The signal reconstruction procedure performed in the LINC combiner is described in equation 2.9, which assumes that each HPA has the same amplification gain [5]. However, when this is not the case it may lead to a significant performance degradation [6, 7]. On that account, this section studies the impact of the gain and phase imbalances between the LINC's HPAs on the performance of the proposed transmission scheme. These impacts are evaluated separately, i.e. each scenario considers either a gain or a phase imbalance.

This study is critical for the design and implementation of the HPAs when a LINC technique is used, like the one inserted in the project GLANCES [16]. The proposed

HPAs to be developed in this context aim to keep the gain imbalances under 0.1dB (i.e. beneath 2%) and the phase imbalances below $0.5°$.

Figure 4.7 illustrates the spectral spreading of the transmitted signal s_c for different gain imbalances Δg, while figure 4.8 assesses the BER performance loss for the same scenarios. As these figures show, the proposed RMM combined with LINC system is fairly insensitive to the studied gain imbalances between the HPAs.

Figure 4.7: Impact of gain imbalance (Δg) on the PSD of the LINC's transmitted signal.
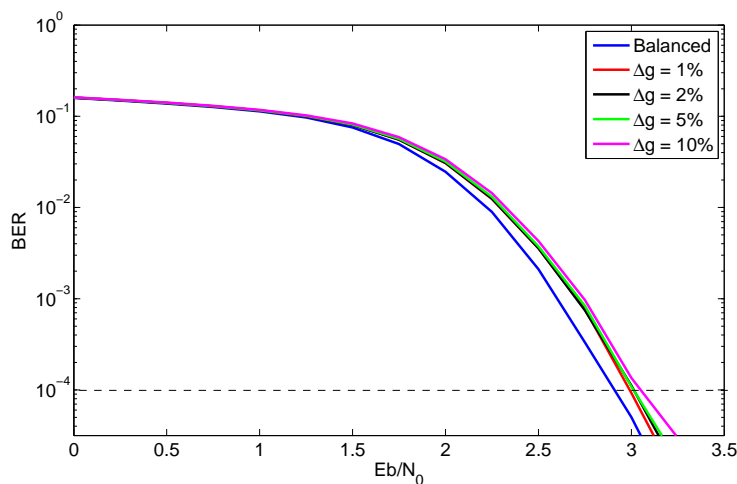
Figure 4.8: Impact of gain imbalance (Δg) in the BER performance on the AWGN channel, for LDPC coded RMM transmission.

On the other hand, the LINC transmitters are typically more sensitive to phase imbalances [6, 7], as it is expected, since the constant-envelope LINC signal components s_{n1} and s_{n2} keep the signal's information in their phases.

Figure 4.9 illustrates the spectral spreading of the transmitted signal s_c for different phase imbalances ϕ, while figure 4.10 assesses the BER performance loss for the same

scenarios. While the BER performance loss is acceptable for $\phi \leq 10°$ (less than 0.5dB for BER$= 10^{-4}$, compared to the balanced case), the PSD's rejection band of the transmitted signal s_c experiences significant spectral regrowth for phase imbalances over $5°$.
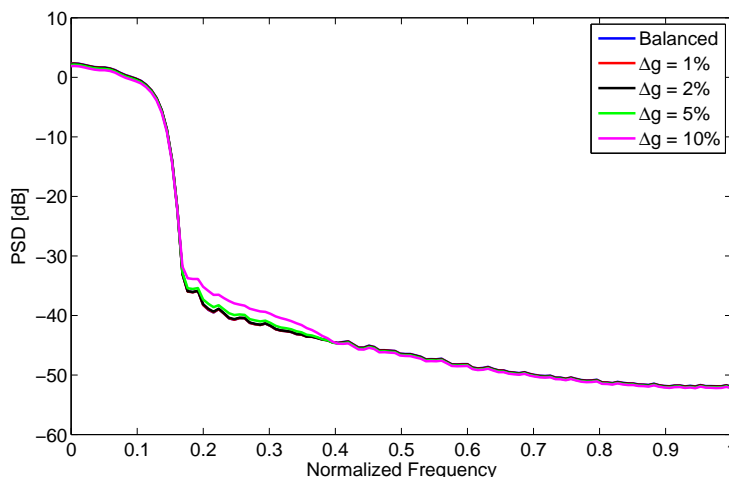

Figure 4.9: Impact of phase imbalance (ϕ) on the PSD of the LINC's transmitted signal.

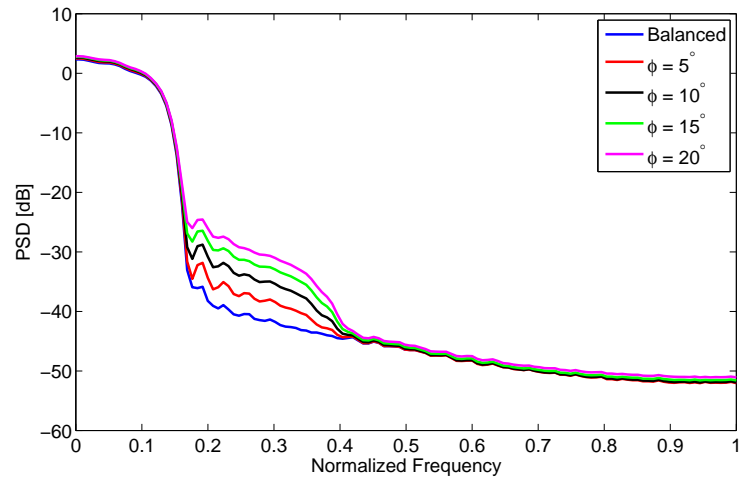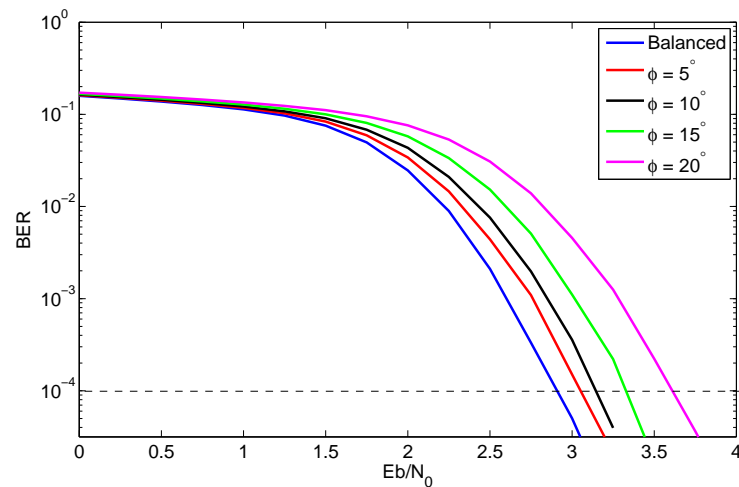Figure 4.10: Impact of phase imbalance (ϕ) in the BER performance on the AWGN channel, for LDPC coded RMM transmission.

44

5

Conclusions

Contents

Projects GALNC [15] and GLANCES [16] focus on the problems associated with the power amplification of high-order constellations signals, that exhibit high envelope excursions, and the linear HPAs' low energy efficiency. Considering the high-order constellations' problem, Dinis *et al.* [26] proved that an M-ary constellation can be decomposed as a sum of several OQPSK signals, to be amplified and transmitted separately.

To overcome the linear HPAs' problem, it is proposed to use a LINC technique [5–7], that achieves high energy efficiency by employing grossly NL HPAs, that are simpler and much more energy efficient. However, the LINC technique has stringent requirements regarding the oversampling rate and the combiner's efficiency, that needed to be solved.

In these projects' context, this thesis work addressed the LINC technique's mentioned requirement problems. On that account, MM techniques were studied to reduce the PAPR of the signal fed to the LINC module. However, despite the good results obtained by combining the MPMM method with the LINC technique that were reported in the paper accepted for oral presentation at VTC Fall[1] 2014 [27] (namely regarding the spectral regrowth of the transmitted signal and the challenges this system faces when the amplifiers' gains are imbalanced), the QPSK modulation scheme was observed to be impractical concerning the mentioned LINC requirements.

After understanding that an OQPSK signal is a much more suited candidate to be amplified using the LINC technique, a new RMM technique was studied and developed regarding offset modulation schemes. Instead of merely limiting the maximum envelope excursions of the transmitted signal, this RMM method also imposes a lower amplitude boundary on the OQPSK signal, which was shown to reduce significantly the spectral enlargement suffered by the LINC signal components. This results in lower oversampling requirements ($L = 8$ enables a simple DAC's reconstruction filter design) and higher combining efficiency (RMM alone increases the combiner's energy efficiency to 63%, but by performing additional post-filtering clipping on the LINC module it is possible to achieve a combiner's efficiency of 76%).

Considering Dinis' work [26], this power amplification technique will be used as a basic amplification unit of more complex transmitter scheme, that employs several of these modules. Therefore, that system will benefit from the proposed scheme's high energy efficiency and the M-ary constellations' high spectral efficiency.

5.1 Future work

The GLANCES project [16] is still on its early stages, and this work will provide the necessary proof of concept upon which the project is built. Since this work addresses

---

[1]See appendix B.

only the transmitter's side of the communication system, the project's next step will be to study an implementation of an iterative block decision feedback equalisation (IB-DFE) receiver [28], specially designed to take into account the developed RMM scheme and the eventual residual amplifier unbalances.

The hardware implementation of the proposed RMM combined with LINC scheme on an FPGA will also be studied, namely regarding the impact of the DAC features (resolution and reconstruction filter) and the signal separation performed by the LINC technique to assess which representation – $e(t)$ or θ – is more adequate, considering each term's computation complexity.

5. Conclusions

Bibliography

[1] S. Miller and R. O'Dea, "Peak power and bandwidth efficient linear modulation," *IEEE Trans. Commun.*, vol. 46, no. 12, pp. 1639–1648, Dec. 1998.

[2] G. Li, Z. Xu, C. Xiong, C. Yang, S. Zhang, Y. Chen, and S. Xu, "Energy-efficient wireless communications: tutorial, survey, and open issues," *Wireless Communications, IEEE*, vol. 18, no. 6, pp. 28–35, December 2011.

[3] S. Zeadally, S. Khan, and N. Chilamkurti, "Energy-efficient networking: past, present, and future," *The Journal of Supercomputing*, vol. 62, no. 3, pp. 1093–1118, 2012.

[4] P. Reynaert and M. Steyaert, *RF Power Amplifiers for Mobile Communications*. Springer, 2006.

[5] D. Cox, "Linear amplification with nonlinear components," *Communications, IEEE Transactions on*, vol. 22, no. 12, pp. 1942–1945, Dec 1974.

[6] A. Birafane, M. El-Asmar, A. Kouki, M. Helaoui, and F. Ghannouchi, "Analyzing LINC systems," *Microwave Magazine, IEEE*, vol. 11, no. 5, pp. 59–71, Aug 2010.

[7] R. Dinis and A. Gusmão, "Nonlinear signal processing schemes for OFDM modulations within conventional or LINC transmitter structures," *European Transactions on Telecommunications*, vol. 19, no. 3, pp. 257–271, 2008.

[8] S. Cripps, "RF power amplifiers for wireless communications," *Microwave Magazine, IEEE*, vol. 1, no. 1, pp. 64–64, Mar 2000.

[9] A. Birafane and A. Kouki, "On the linearity and efficiency of outphasing microwave amplifiers," *Microwave Theory and Techniques, IEEE Transactions on*, vol. 52, no. 7, pp. 1702–1708, July 2004.

[10] S. Litsyn, *Peak Power Control in Multicarrier Communications*. Cambridge University Press, 2007, cambridge Books Online. [Online]. Available: http://dx.doi.org/10.1017/CBO9780511618383

Bibliography

[11] A. Ambroze, M. Tomlinson, and G. Wade, "Magnitude modulation for small satellite earth terminals using QPSK and OQPSK," in *Communications, 2003. ICC '03. IEEE International Conference on*, vol. 3, May 2003, pp. 2099–2103 vol.3.

[12] M. Gomes, "Magnitude modulation for peak power control in single carrier communication systems," Ph.D. dissertation, Universidade de Coimbra, Portugal, 2010.

[13] M. Gomes, F. Cercas, V. Silva, and M. Tomlinson, "Magnitude modulation for VSAT's low back-off transmission," *Journal Commun. Networks (JCN), special issue on Recent Adv. in Satell. and Space Commun.*, vol. 12, no. 6, pp. 544–557, Dec. 2010.

[14] http://www.mathworks.com/products/matlab/.

[15] GALNC "Generalized Linear Amplification with Nonlinear Components for broadband wireless systems" EXPL/EEI-TEL/1582/2013 — Projecto Exploratório FCT.

[16] http://www.it.pt/project_detail_p.asp?ID=1939.

[17] M. Gomes, V. Silva, A. Simões, R. Dinis, and P. Montezuma, "Method and system to perform ring-type envelope control of offset-modulation signals with limited bandwidth," Provisional application for patent, 2014.

[18] ——, "LINC transmitter with improved efficiency foroffset-modulation signals with limited bandwidth," Provisional application for patent, 2014.

[19] L. Sundstrom, "The effect of quantization in a digital signal component separator for LINC transmitters," *Vehicular Technology, IEEE Transactions on*, vol. 45, no. 2, pp. 346–352, May 1996.

[20] S. A. Hetzel, A. Bateman, and J. McGeehan, "A LINC transmitter," in *Vehicular Technology Conference, 1991. Gateway to the Future Technology in Motion., 41st IEEE*, May 1991, pp. 133–137.

[21] F. J. Harris, *Multirate Signal Processing for Communication Systems*. Prentice Hall PTR, 2004.

[22] M. Gomes, V. Silva, F. Cercas, and M. Tomlinson, "Power efficient back-off reduction through polyphase filtering magnitude modulation," *Communications Letters, IEEE*, vol. 13, no. 8, pp. 606–608, August 2009.

[23] S. K. Mitra, *Digital Signal Processing: A Computer Based Approach - 3th ed.* McGraw-Hill, 2006.

[24] *Digital Video Broadcasting (DVB); Second generation framing structure, channel coding and modulation systems for Broadcasting, Interactive Services, News Gathering and other broadband satellite applications*, ETSI Std. EN 302 307 V1.3.1, Mar. 2013.

[25] S. Lin and J. D. J. Costello, *Error Control Coding, 2nd ed.*   NJ: Pearson Prentice Hall, 2004.

[26] R. Dinis, P. Montezuma, N. Souto, and J. Silva, "Iterative frequency-domain equalization for general constellations," in *Sarnoff Symposium, 2010 IEEE*, April 2010.

[27] A. Simões, M. Gomes, R. Dinis, V. Silva, and F. Cercas, "Magnitude modulation applied to LINC transmitters: Paving the road for better efficiency," *IEEE 80th Vehicular Technology Conference: VTC2014-Fall*, Sep 2014.

[28] N. Benvenuto, R. Dinis, D. Falconer, and S. Tomasin, "Single carrier modulation with nonlinear frequency domain equalization: An idea whose time has come again," *Proceedings of the IEEE*, vol. 98, no. 1, pp. 69–96, jan. 2010.

[29] E. Lee and D. Messerschmitt, *Digital Communication*.   Springer Netherlands, 1988.

[30] J. G. Proakis, *Digital Communications - 4th ed.*   McGraw-Hill, 2000.

[31] A. Carlson and P. Crilly, *Communication Systems*.   McGraw-Hill, 2009.

Bibliography

A

QPSK and OQPSK Digital Modulators

A. QPSK and OQPSK Digital Modulators

This section briefly describes the QPSK and OQPSK modulation schemes, providing only the necessary insight to fully understand the proposed transmission scheme[1]. This analysis considers signals with unitary average power, for simplicity. Figure A.1 illustrates a typical symbol mapping by such modulators, when using Gray coding.
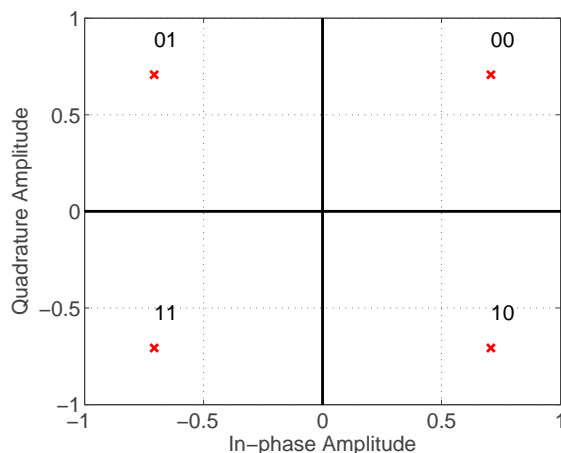

Figure A.1: QPSK and OQPSK Gray coded constellation, with unitary average power.

A generic SC transmission system using an OQPSK modulator is depicted in Figure A.2 [31]. This figure shows that although both modulation schemes map a given bitstream the same way, the corresponding transmitted signal is different[2]. Equation A.1 gives the sample values of such schemes (with an even oversampling factor L):

$$s[n] = s^I[n] + s^Q\left[n - k\frac{L}{2}\right] , \qquad (A.1)$$

where s^I and s^Q represent the in-phase and quadrature signal components, respectively, while $k = 0$ and $k = 1$ distinguishes between QPSK and OQPSK digital modulation schemes. By offsetting the timing of the in-phase and quadrature signal components by half a symbol period, the transmitted signal's envelope excursions are smaller, since the components' peak values occur at different moments.

---

[1]A thorough theoretical BER and spectrum analysis is easily found in the literature [29, 30].

[2]A SC transmission system using a QPSK modulator does not delay the signal's quadrature component by half a symbol duration $\frac{T_{symb}}{2}$ (here represented by $\frac{L}{2}$).
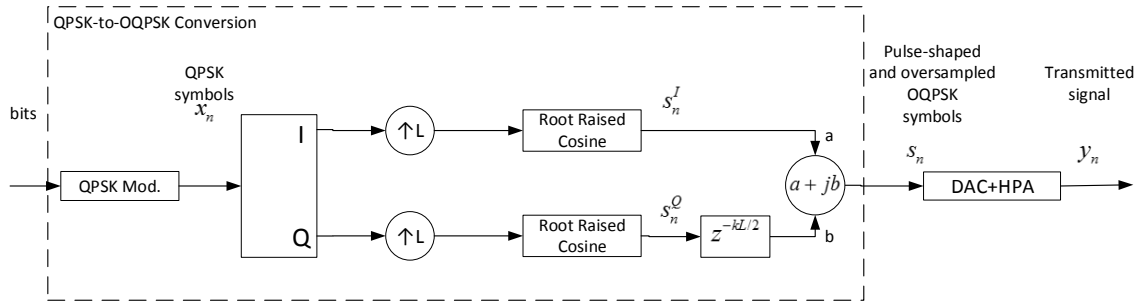
Figure A.2: Generic single-carrier transmitter scheme, performing OQPSK modulation using a QPSK modulator, a generic pulse shaping filter and even oversampling factor.

Besides removing the undesirable zero-crossings from the OQPSK's diagram of the transition paths between the constellation's symbols, this timing offset also results in a maximum phase-shift of $90°$ for this constellation (instead of the $180°$ phase-shifts that can occur with a QPSK signal). This can be seen in the following transition path diagrams:
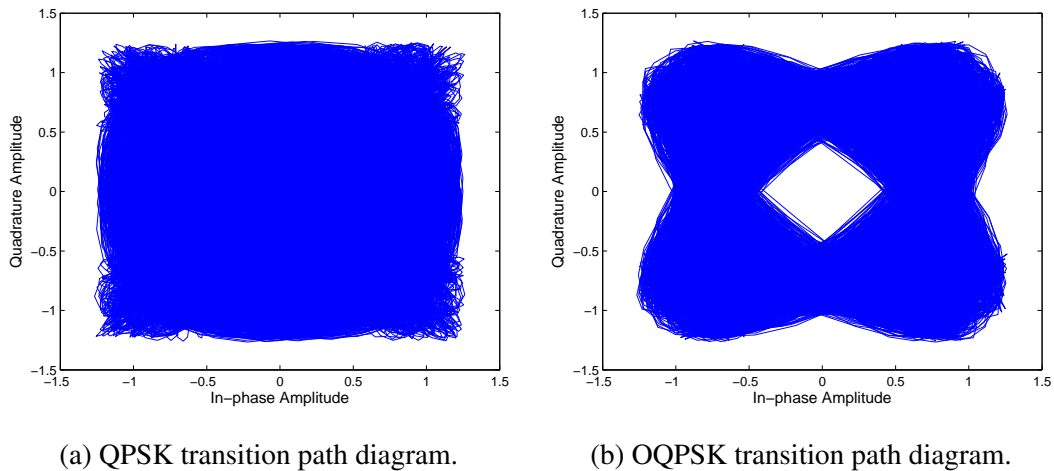
(a) QPSK transition path diagram.

(b) OQPSK transition path diagram.

Figure A.3: Diagrams of the transition paths between the constellation's symbols of transmitted signals in typical SC transmitter schemes using QPSK and OQPSK digital modulators, respectively, using an RRC filter with a 25% roll-off factor and an oversampling factor $L = 8$.

Another important assessment comes from figure A.4, that shows a typical time variation of the QPSK and OQPSK signal envelopes[3]. The OQPSK signal has a more controlled envelope excursions that an equivalent QPSK modulated signal, as shown:

---

[3]The transition path diagram A.3b may give the wrong impression about the OQPSK samples' amplitude values nearby the constellations' symbol positions.

(a) QPSK signal.

(b) OQPSK signal.
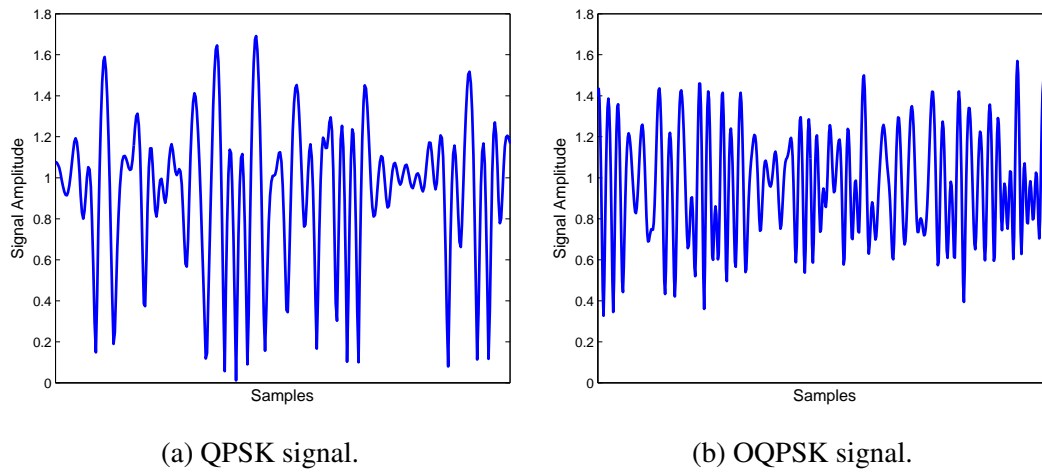
Figure A.4: Time variation of the amplitude of the transmitted signals in typical SC transmitter schemes employing QPSK and OQPSK digital modulation schemes, respectively.

Since there is only a time-shift between the in-phase and quadrature components, it is clear that both modulation schemes have the same bandwidth [29, 30], as illustrated in figure A.5.
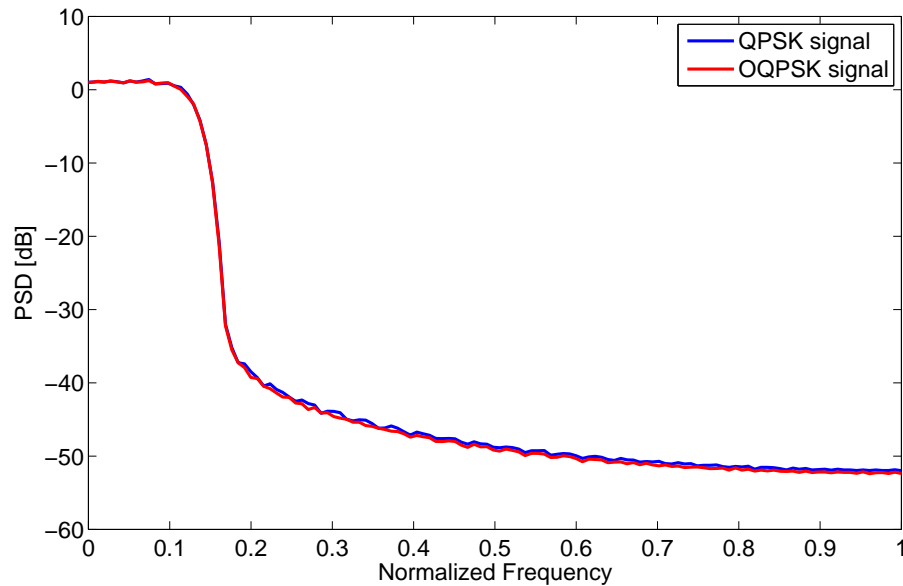

Figure A.5: PSD of equivalent QPSK and OQPSK signals..

B

Accepted paper at IEEE VTC Fall 2014

Magnitude Modulation applied to LINC transmitters: Paving the Road for Better Efficiency

António Simões*†, Marco Gomes*†, Rui Dinis*‡, Vitor Silva*† and Francisco Cercas*§

*Instituto de Telecomunicações, Portugal
†Department of Electrical and Computer Engeneering, University of Coimbra, 3030-290 Coimbra, Portugal
‡FCT-UNL, 2829-516 Caparica, Portugal, §ISCTE-IUL, 1649-026 Lisbon, Portugal

Abstract—The linear amplification with nonlinear components (LINC) amplification concept is very important on the developing of the modern mobile and satellite communications systems due to the use of inexpensive high power amplifiers (HPA). This paper analyses the effectiveness of combining an efficient PAPR reducing technique based on magnitude modulation (MM) when applied to a LINC amplification system. The simulation results show that the inclusion of the MM on the LINC processing chain is very favourable in terms of spectral regrowth introduced by signal's clipping distortion. The system is also more robust to gain and phase imbalances between amplifiers with only a marginal bit error rate (BER) loss for an uncoded transmission scenario.

Index Terms—LINC, HPA, PAPR, Magnitude Modulation

I. Introduction

The rising demand for spectral and power efficiency in communication systems, namely on mobile devices, makes the study of low peak-to-average power ratio (PAPR) signals worthy of attention, due to the lower requirements of back-off from the high power amplifier (HPA) saturation point [1]–[4]. The HPA is one of the critical components in the design of wireless transmitters, to which most spectral efficient transmission techniques impose stringent linearity require-ments (i.e., the use of class A or AB power amplifiers or quasi-linear amplifiers) with a consequent negative impact on power efficiency (e.g., class A power amplifiers' efficiency is below 20%) and HPA's cost. With this in mind, the use of a linear amplification with non-linear components (LINC) [5]–[7] transmission scheme becomes attractive, since this structure separates the input signal in two constant-envelope branches to be amplified separately by two highly efficient grossly nonlinear (NL) amplifiers (e.g., class D and E am-plifiers, whose efficiencies reach 80%), which are simpler, cheaper and have higher amplification and output power than quasi-linear amplifiers [4], [8]. A linear amplified replica of the input signal is obtained by combining the two amplified component signals as long as the amplifiers are perfectly matched (i.e. without gain and phase imbalances between each other) [5], [6] and have sufficient bandwidth to accommodate each LINC component signal. Current LINC combiners have 50% power efficiency, which gives the overall system a 40% power efficiency, largely above the mentioned 20% threshold obtained with linear power amplifiers. Besides distortions due

to imperfect combining, the LINC scheme may also involve amplitude clipping due to input power limitations of the component amplifiers, which would result in additional high frequency distortion (i.e. spectral regrowth) on the transmitted signal.

To avoid the mentioned distortion, the signal should remain below the amplitude clipping level as often as possible. But we should not fear this clipping level, since it can provide an important tradeoff between power and spectral efficiency when used with caution.

Caution brought us back to the signals' high peak power problem, but this time for a different reason. Suppressing the peaks from the transmitted signal would result in fewer signal amplitude clipping occurrences, which would mitigate the undesirable high frequency distortion that it adds on the reconstructed signal. In this context, magnitude modulation (MM) [9]–[11] seems to be a good fit, since a controlled signal envelope gives extra room to vary the amplitude clipping level with unnoticeable transmission performance reduction.

On the study of generalised LINC systems for future broad-band wireless systems efficient in both power and bandwidth [12], the combining of MM techniques with LINC systems surges as a natural reasoning. In this paper we present some initial results on the impact of the polyphase magnitude mod-ulation [10], [11] scheme on the LINC transmission system. This real-time peak reduction method is simple to implement, since it only depends on the system's pulse shaping filter impulse response (typically a root-raised cosine (RRC) filter with finite impulse response [13]), making this an effortless, as well as robust, mean to improve the transmission spectral efficiency.

To evaluate the proposed transmission scheme we use the QPSK constellation. The results show that there is an optimal amplitude clipping level for the LINC system when combined with MM techniques where we can make the best out of the mentioned tradeoff. We also examine the system's performance when facing gain and phase imbalances in the two LINC branches' power amplifiers [8]. For comparison purposes, we also evaluate the performance of a LINC trans-mission scheme without MM.

This paper is organized as follows. Section 2 presents the proposed system (combination of MM with LINC), where we will discuss how to make the best of this MM approach. The performance of each scheme is analysed in section 3. Section 4 evaluates the effect of phase and gain imbalances in both
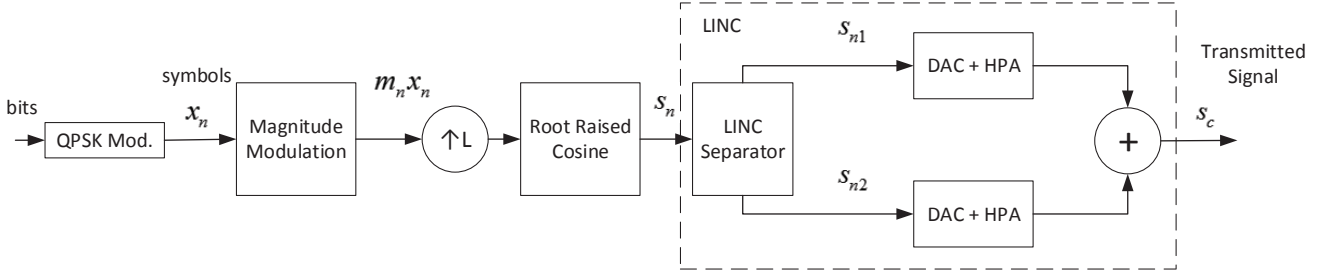
Fig. 1. Block diagram of combined MM with LINC system.

schemes. Finally, section 5 summarises the main conclusions.

II. COMBINING MM WITH LINC

Figure 1 illustrates the basic building blocks of the combined MM with LINC transmission system. As in [10], [14], the system takes into account the pulse shaping RRC filter coefficients along with past and future symbols (in this case, mapped into a QPSK constellation, with Gray coding) around each data pulse, and thus the MM block can prevent any peak occurrences on the LINC input signal beyond a certain amplitude level A. The signal s_n at the input of the LINC system can be written as

$$s_n = \sum_k m_k x_k h_{n-k} \ , \tag{1}$$

where x_n is the modulated symbols' sequence, m_n the respective sequence of multiplying MM factors and h_n the impulse response of the pulse shaping filter.

Different schemes can be used to compute the MM factors, with the most common being the MM LUT-based implementation [9], [14] with MM factors being computed a priori, and the multistage polyphase magnitude modulation (MPMM) technique [10], [14] that computes MM coefficients in real time based on a low complexity polyphase filter system. Both algorithms compute m_n in order to guarantee that

$$|s_n| \le A, \tag{2}$$

It [15] has been shown that MM factors, m_n, for constant amplitude constellations follow a beta distribution, i.e.

$$p(m) = \frac{\Gamma(\alpha+\beta)}{\Gamma(\alpha)\Gamma(\beta)} m^{\alpha-1}(1-m)^{\beta-1} \ , \tag{3}$$

with α and β being dependent on modulation order and the RRC filter roll-off, whereby the complementary cumulative distribution function (CCDF) of the PAPR of (1) can be obtained. Fig. 2 presents the CCDF of the PAPR of a MM QPSK signal, where potential margin for gain in power efficiency is clear.

The magnitude modulated pulse shaped signal s_n is fed to LINC analysis system which performs a signal separation operation on its input signal, in two constant envelope amplitude signals given by [5]–[7]:

$$s_{n1} = f_1\left(|s_n|\right)\exp\left(j\arg\left(s_n\right)\right) \ , \tag{4}$$

$$s_{n2} = f_2\left(|s_n|\right)\exp\left(j\arg\left(s_n\right)\right) \ , \tag{5}$$

with

$$f_1(R) = f_c(R) + j f_e(R) \ , \tag{6}$$

$$f_2(R) = f_c(R) - j f_e(R) \ , \tag{7}$$

where, $f_c(R)$ and $f_e(R)$ perform the polar clipping operation as follows

$$f_c(R) = \begin{cases} \frac{1}{2}R, & R \le s_M \\ \frac{1}{2}s_M, & R > s_M \end{cases} \ , \tag{8}$$

$$f_e(R) = \begin{cases} \frac{1}{2}\sqrt{s_M^2 - R^2}, & R \le s_M \\ 0, & R > s_M \end{cases} \ , \tag{9}$$

where s_M is the clipping level of the LINC system. This polar clipping operation was chosen over the Cartesian type due to its slightly superior performance, [7]. A simple analysis confirms that both branches have equal and constant amplitude $\frac{s_M}{2}$, allowing us to include two grossly nonlinear amplifiers on our transmission system without distortion. These amplifiers are inexpensive and much more energy-efficient than the linear ones [4], [8].

Assuming ideally balanced amplifiers and perfect combining, we can determine the transmitted signal using the following equation (where we assume an amplifiers' unit power gain):

$$s_c = s_{n1} + s_{n2} = \begin{cases} s_n, & |s_n| \le s_M \\ s_M \exp\left(j\arg\left(|s_n|\right)\right), & |s_n| > s_M \end{cases} . \tag{10}$$
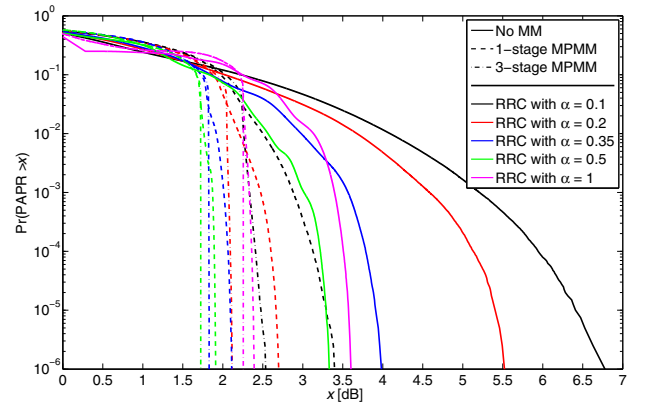

Fig. 2. CCDF of the PAPR for bandwidth limited QPSK transmission.

This shows that the combination of the two branches can perfectly reverse the LINC's separation nonlinear operation as long as the entire signal stays below the clipping level, and the HPAs in each branch are balanced and can accommodate the resulting signals entire spectrum. But for transmission systems that do not require perfect reconstruction, the clipping level can be explored to improve the power efficiency of the transmission system without adding too much distortion, as long as the signal is not clipped very often. This is the key idea behind our MM approach to a LINC transmission system, as we will be discussing next.

A. Optimum clipping level

We start this subsection by comparing the LINC input signal with and without the use of MM that we denote by $\tilde{s}_n$ and s_n, respectively. For comparison's sake, each system is designed in such a way that in both cases the signal fed to the LINC separator has unitary average power. Since there is a clipping operation inside the LINC separator, the logical first step is to determine the probability of $|s_n|$ crossing the defined level s_M, to empirically assess their respective performance degradation.

As we have mentioned before, we have been working with a clipping level s_M since the s_n complex signal fed to the LINC separator has unitary average power. However, we can broaden our analysis by defining instead a clipping ratio $\frac{s_M}{\sigma_s}$, where $\sigma_s^2 = E[|s_n|^2]$.

Fig. 3 illustrates both input signals' cumulative distribution functions (CDFs). As long $|\tilde{s}_n|$'s CDF curve remains above the CDF of $|s_n|$, i.e. as long as the magnitude modulated signal $\tilde{s}_n$ suffers less clipping than s_n, there is an opportunity to use with advantage the combined MM+LINC system. Considering that to avoid severe clipping distortion on the LINC separation, the signal must not be clipped very often, there is a favourable region where the clipping level should be chosen as indicated in Fig. 3.
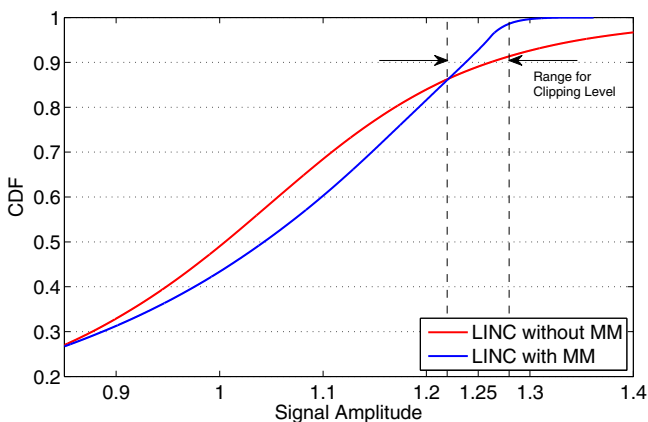
III. Simulation Results

A. The LINC structure's oversampling requirements

We start this section by analysing one particular limitation of the discrete time LINC system implementation: its oversampling requirements. As we can see by looking at the LINC branches' equations (4)–(9), their constant envelope is obtained by phase modulation, a nonlinear function of the input signal's amplitude $|s_n|$. This nonlinearity produces spectral regrowth, when comparing the spectrums of components s_{n1} and s_{n2} with the one of s_n, consistent with the wide characteristic of the spectrum of a constant envelope signal [6]. This demands for a digital LINC system working at a higher rate. Fig. 4 shows one of the branches power spectrum density (PSD) for different oversampling ratio L (considering unitary average power for all cases) of the LINC separator. This particular simulation did not involve clipping, so we could correctly make an empirical evaluation of the oversampling's effect on the LINC branches.

The same conclusions can be drawn from analysis of Fig. 5. It depicts the ideal amplitude's CDF of the analog signal component s_{n1} (that was obtained through simulation of a reconstruction system with an excessive oversampling
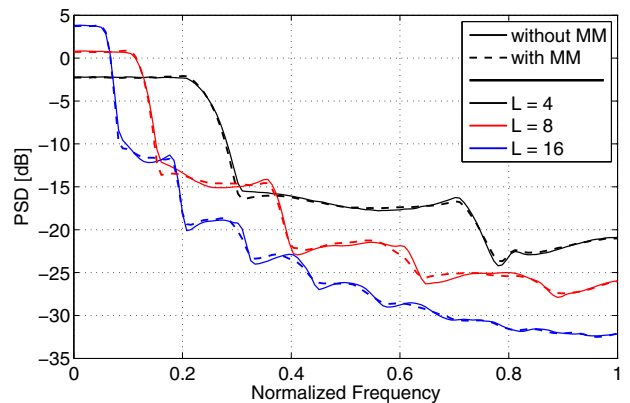

Fig. 4. LINC branch's PSD for different oversampling factors L, with and without MM.

Fig. 3. CDF of the LINC's input signal with and without MM envelope control.
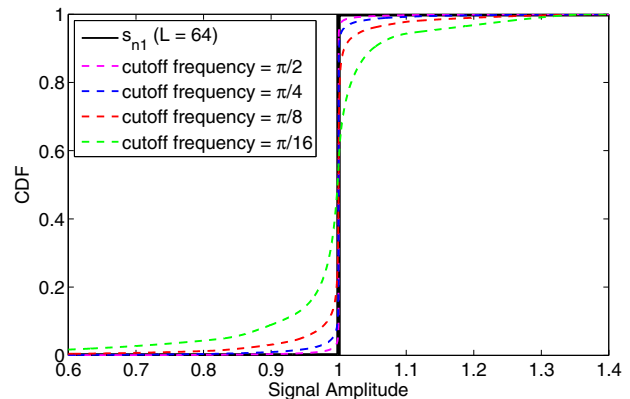

Fig. 5. CDF of the s_{n1} component calculated with an excessive oversampling ratio ($L = 64$) and the effect of the DAC's limited bandwidth reconstruction filter on the amplitude of the transmitted analog component.
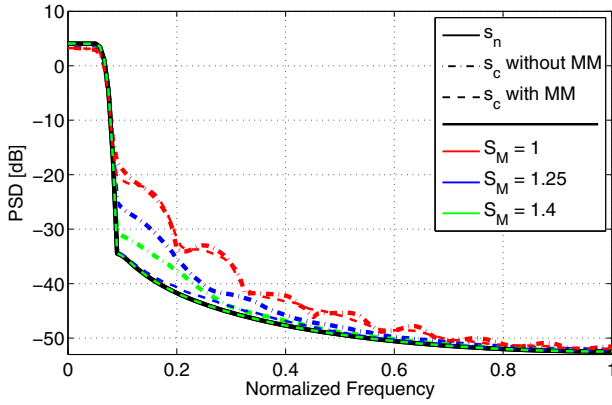
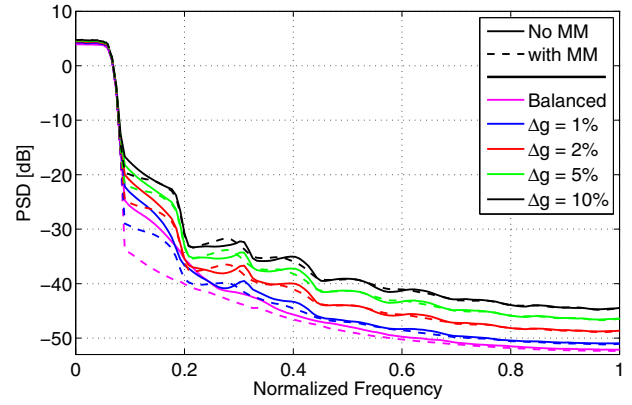Fig. 6. PSD of the LINC input signal s_n vs PSD of the transmitted signal s_c with and without MM.

Fig. 8. Impact of gain imbalance (Δg) on the PSD of the LINC's transmitted signal.
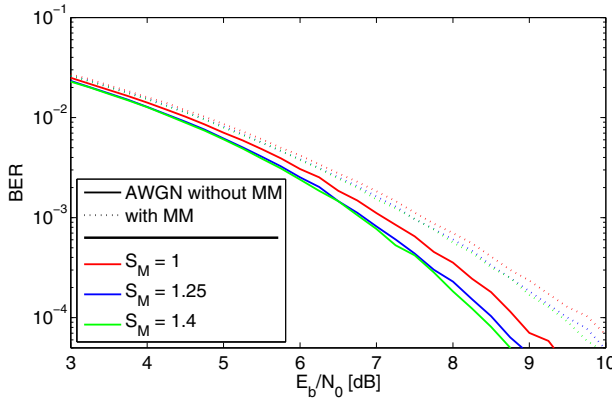

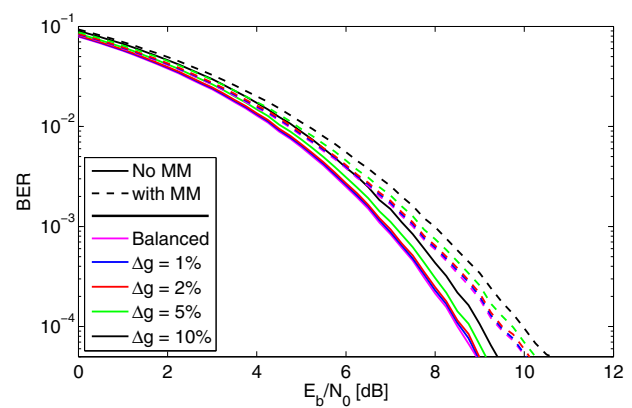Fig. 7. BER performance of uncoded QPSK LINC transmission over an AWGN channel.

Fig. 9. Impact of gain imbalance (Δg) in the BER performance on the AWGN channel, for an uncoded transmission.

frequency), and compares it with the amplitude's CDF for different band limited signals, due to the reconstruction filter effect of a digital to analog converter (DAC) operating at a lower rate.

Results show the necessity of using a high level of over-sampling in order to ensure that the reconstruction filter of the DAC conversion of both LINC branches does not destroy the constant envelope characteristic of s_{n1} and s_{n2} signals. In addition, this also shows the requirement for using on LINC perfectly matched NL amplifiers with sufficient bandwidth to accommodate each signal's component. It is important to note that this bandwidth is much larger than the one an LINC's equivalent quasi-linear amplifier.

B. PSD and BER

We focus now on the analysis of the results shown in Fig.s 6 and 7, where we compare combined MM+LINC with basic LINC for different clipping levels, in terms of the PSD of the reconstructed LINC output signal s_c (see eq. (10)) and the BER performance of transmitting uncoded s_c mapped in a QPSK constellation (with Gray coding) over an AWGN channel. In the simulations we considered $L = 16$, and 1-stage polyphase MM system [10] designed for a 0.2 roll-off RRC filter.

When the clipping level is 1.4, the basic LINC's input signal gets clipped (although not very often), but the magnitude modulated signal is decomposed on LINC without being clipped (see Fig. 3). In this case, the amount of distortion caused by clipping the basic LINC's input signal is limited to a 4 dB spectral regrowth in the rejection band.

However, when setting the clipping to level 1.25, inside the favourable region defined in Fig. 3, the difference between the basic and MM+LINC reconstructed signals' rejection band increases to a noteworthy 9dBs. Both signals get clipped in this case, but the magnitude modulated signal clipping happens much less frequently than in the other signal ($4 - 5\%$ less, according to the CDF in Fig. 3). This clipping level is near the optimal solution, where the magnitude modulated signal's PSD have significantly less out of band spectral regrowth than in the other scenario. When comparing BER of both systems, for an uncoded transmission, the degradation is only about 1dB. However, this loss vanishes since typical systems always employ channel coding, with MM distortion being absorbed by the error correcting capabilities of the used channel coding solution [10], [14].

Thus, when considering a LINC application with bandwidth scarcity, magnitude modulation is an effortless and viable
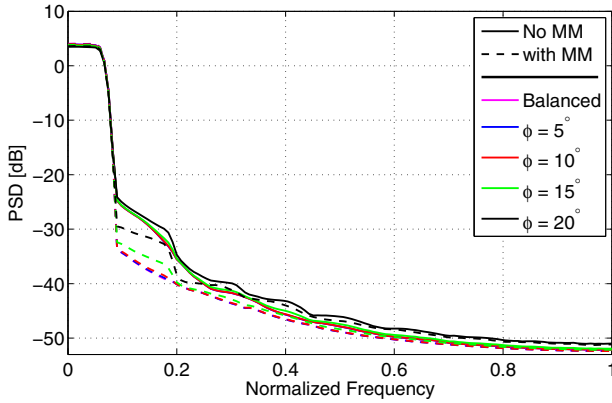
Fig. 10. Impact of phase imbalance (ϕ) on the PSD of the LINC's transmitted signal.
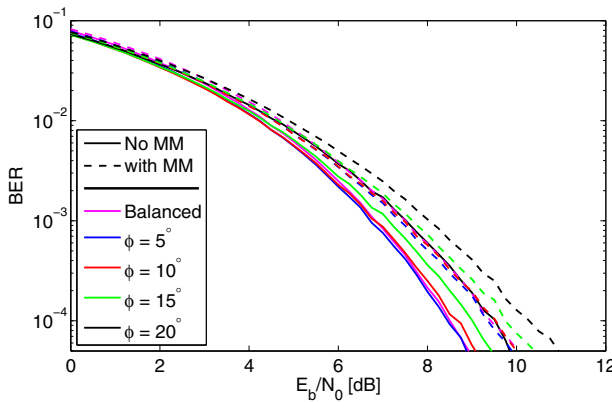

Fig. 11. Impact of phase imbalance (ϕ) in the BER performance on the AWGN channel, for an uncoded transmission.

solution, guaranteeing performance while improving spectral behaviour.

Finally, we observe that setting the clipping level to 1 is too harsh on both signals, since more than half of their samples suffer amplitude clipping. They experience similar spectral regrowth, which makes the performance degradation unacceptable.

IV. Impact of Gain and Phase Imbalances in the Combined MM with LINC Scheme

In this section we analyse the robustness of the combined MM+LINC system when facing gain or phase imbalances between its two branches' power amplifiers. For this analysis we set the LINC's amplitude clipping level at 1.24 (which exhaustive simulation results have shown to be the optimal value from the range mentioned in section II-A).

Fig. 8 illustrates the transmitted signal PSD in both systems, comparing the ideal, i.e. balanced case, to a set of gain imbalances. As we can see, both systems' PSD experience spectral regrowth in their rejection bands from these gain imbalances, meaning that such systems tolerates a maximum 1% gain imbalance. It is however noteworthy that the combined LINC+MM systems still perform much better than the

conventional LINC. When analysing the BER results shown in Fig. 9 we observe that both systems can handle up to 5% gain imbalance without noticeable performance loss.

Finally, we conclude in a similar manner from the results reported in Fig.s 10 and 11 that the system branches' phase imbalance can reach up to 10 degrees without adding a significant amount of distortion to the transmitted signal.

V. Conclusions

This work explores the introduction of the MM technique in the processing chain of a LINC system in order to combat the spectral regrowth of the transmitted signals due to signal clipping and imbalances of non-ideal amplifiers. The carried out simulations have shown very interesting results in terms of the power spectrum and BER. In the near future, this work will be significantly improved in the context of a wide research project on generalized LINC systems for future broadband wireless communications systems.

References

[1] S. Miller and R. O'Dea, "Peak power and bandwidth efficient linear modulation," *IEEE Trans. Commun.*, vol. 46, no. 12, pp. 1639–1648, Dec. 1998.

[2] G. Li, Z. Xu, C. Xiong, C. Yang, S. Zhang, Y. Chen, and S. Xu, "Energy-efficient wireless communications: tutorial, survey, and open issues," *Wireless Communications, IEEE*, vol. 18, no. 6, pp. 28–35, December 2011.

[3] S. Zeadally, S. Khan, and N. Chilamkurti, "Energy-efficient networking: past, present, and future," *The Journal of Supercomputing*, vol. 62, no. 3, pp. 1093–1118, 2012.

[4] P. Reynaert and M. Steyaert, *RF Power Amplifiers for Mobile Communications*. Springer, 2006.

[5] D. Cox, "Linear amplification with nonlinear components," *Communications, IEEE Transactions on*, vol. 22, no. 12, pp. 1942–1945, Dec 1974.

[6] A. Birafane, M. El-Asmar, A. Kouki, M. Helaoui, and F. Ghannouchi, "Analyzing linc systems," *Microwave Magazine, IEEE*, vol. 11, no. 5, pp. 59–71, Aug 2010.

[7] R. Dinis and A. Gusmão, "Nonlinear signal processing schemes for ofdm modulations within conventional or linc transmitter structures," *European Transactions on Telecommunications*, vol. 19, no. 3, pp. 257–271, 2008.

[8] S. Cripps, "Rf power amplifiers for wireless communications," *Microwave Magazine, IEEE*, vol. 1, no. 1, pp. 64–64, Mar 2000.

[9] A. Ambroze, M. Tomlinson, and G. Wade, "Magnitude modulation for small satellite earth terminals using qpsk and oqpsk," in *Communications, 2003. ICC '03. IEEE International Conference on*, vol. 3, May 2003, pp. 2099–2103 vol.3.

[10] M. Gomes, V. Silva, F. Cercas, and M. Tomlinson, "Power efficient back-off reduction through polyphase filtering magnitude modulation," *Communications Letters, IEEE*, vol. 13, no. 8, pp. 606–608, August 2009.

[11] M. Gomes, R. Dinis, V. Silva, F. Cercas, and M. Tomlinson, "Error rate analysis of m-psk with magnitude modulation envelope control," *Electronics Letters*, vol. 49, no. 18, pp. 1184–1186, August 2013.

[12] http://www.it.pt/project_detail_p.asp?ID=1939.

[13] J. G. Proakis, *Digital Communications - 4th ed.* McGraw-Hill, 2000.

[14] M. Gomes, F. Cercas, V. Silva, and M. Tomlinson, "Magnitude modulation for VSAT's low back-off transmission," *Journal Commun. Networks (JCN), special issue on Recent Adv. in Satell. and Space Commun.*, vol. 12, no. 6, pp. 544–557, Dec. 2010.

[15] M. Gomes, V. Silva, F. Cercas, and M. Tomlinson, "Analytical analysis of polyphase magnitude modulation method's performance," in *Proc. IEEE ICC'2010*, Cape Town, South Africa, May 2010.